Solid-State Chemistry

DOI: 10.1002/anie.200906780

Ab Initio Thermochemistry of Solid-State Materials

*Ralf Peter Stoffel, Claudia Wessel, Marck-Willem Lumey, and Richard Dronskowski**

Keywords:
density functional calculations · phonons · solid-state chemistry · thermochemistry · transition states

Dedicated to Professor Arndt Simon on the occasion of his 70th birthday

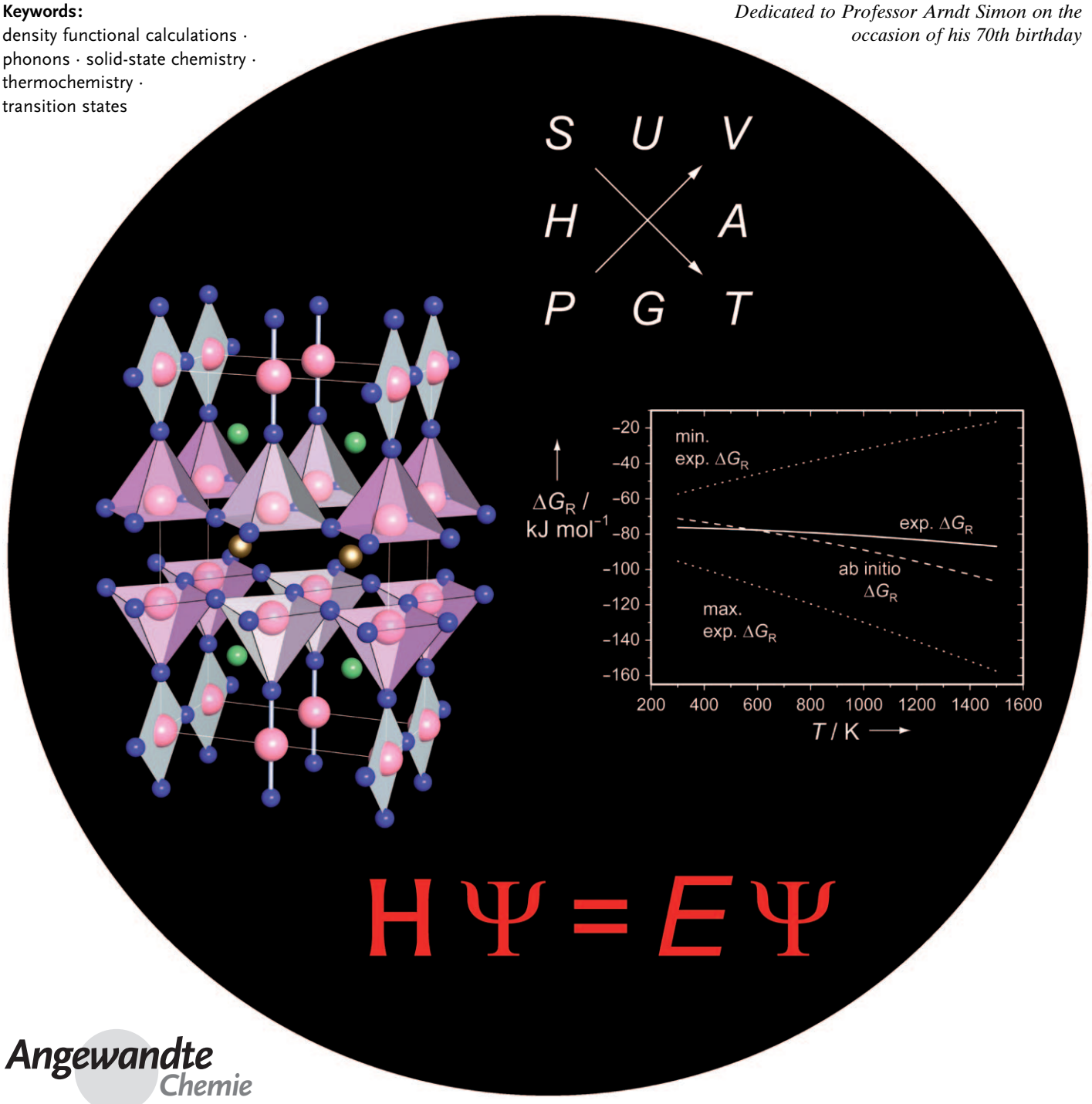

In this contribution we introduce an electronic-structure-theory-based approach to a quantum-chemical thermochemistry of solids. We first deal with local and collective atomic displacements and explain how to calculate these. The fundamental importance of the phonons, their dispersion relations, their experimental determination as well as their calculation is elucidated, followed by the systematic construction of the thermodynamic potentials on this basis. Subsequently, we provide an introduction for practical computation as well as a critical analysis of the level of accuracy obtainable. We then show how different solid-state chemistry problems can be solved using this approach. Among these are the calculation of activation energies in perovskite-like oxides, but we also consider the use of theoretical vibrational frequencies for determining crystal structures. The pressure and temperature polymorphism of elemental tin which has often been classically described is also treated, and we energetically classify the metastable oxynitrides of tantalum. We also demonstrate, using the case of high-temperature superconductors, that such calculations may be used for an independent evaluation of thermochemical data of unsatisfactory accuracy. Finally, we show the present limits and the future challenges of the theory.

From the Contents

1. Introduction 5243
2. Classical Thermochemistry 5244
3. Temperature-Dependent Atomic Displacements 5246
4. Principle Approach 5250
5. Practical Implementation 5253
6. Solutions of Different Solid-State and Materials Chemistry Problems 5256
7. Outlook 5262

1. Introduction

It may well be argued whether or not it does a chemical discipline a great injustice to take the discipline's self-chosen motto much too literally, but German solid-state chemistry would insist that its motto, the proud PERENNE NIL NISI SOLIDUM ("nothing is everlasting unless it is solid") is just as meaningful an assessment as this very science. In the long run, only the solid really has constancy, and this resistance of solid-state materials, their practically nonexistent volatility, their well-ordered structures, and their (at least at room temperature) hardly existent reactivity—exceptions prove the rule—are undoubtedly attributes that some outsiders associate directly with solid-state chemistry.[1–4] Now it is undoubtedly true that, even at the beginning of the 21st century, broad regions of this discipline are still naturally and primarily busy with preparative and crystallographic problems, and this with in part startling successes. Ever new classes of novel solids (e.g., intermetallics, nitrogen-based, nanostructures) with fantastic physical properties (magnets, phosphors, catalysts, superconductors, etc.) are reported,[5] and modern quantum-chemical—as a rule still "static"—calculations allow subsequent deep insights into the structure and bonding of these substances.

On the other hand, it is remarkable how, even today, important questions about the *dynamics* of solids, their chemical reactivity and their reaction mechanisms do not receive the desirable attention, although for the fundamental meaning of *thermodynamic quantities* in solid-state chemistry—is it a stable or unstable compound?—there is not the smallest doubt. As early as 1926 Tammann published in this very journal, then still titled *Zeitschrift für Angewandte Chemie*, a first, weighty and pioneering article about the reactivity of solids,[6] and the rule named after him makes it known that the temperature of solid–solid reactions with respect to the melting or decomposition temperature of the lighter "volatile" component can be predicted at least semi-quantitatively. Naturally the temperature also played an outstanding role in later solid-state chemistry monographs by Hedvall,[7] Hauffe,[8] and Schmalzried,[9] and these contributions either were of an empirically observing nature or used purely classical models. One result of this Review is that at the beginning of the 21st century, exactly 84 years after Tammann, a complete non-classical modeling of practically any complex solid has become possible, which, on the one hand, allows sufficiently high accuracy and, on the other hand, because of the quantum-chemical and no longer classical approach, also correctly describes the "materiality" of the compounds.

For the chemistry itself, a little modesty is initially appropriate: interestingly, the significance of thermochemistry was recognized in the neighboring discipline of metals research very early,[10] and indeed for good reason: the major area of application of this particular science, which is clearly reflected in the necessity for establishing complicated intermetallic phase diagrams, the rational production of steel, the thermochemical description of slags, the high-temperature

[*] R. P. Stoffel, C. Wessel, Dr. M.-W. Lumey, Prof. R. Dronskowski
Institut für Anorganische Chemie, RWTH Aachen University
52056 Aachen (Germany)
E-mail: drons@HAL9000.ac.rwth-aachen.de

corrosion, as well as other practical issues, probably influenced the development of quantitative thermochemistry much stronger[11] than other disciplines could, including chemistry. To connect the quantitative classical modeling tools of thermochemistry with modern electron-theory methods, we must first return to those same classical approaches.

2. Classical Thermochemistry

"*The whole is simpler than the sum of its parts.*" (Josiah Willard Gibbs)

2.1. Thermodynamic Potentials and Databases

Since the fundamental works by Gibbs at the end of the 19th century,[12] practically the entire mathematical apparatus for the quantitative description of classical thermochemistry is available. The so-called Gibbs energy (or free enthalpy), G, represents the "most general" thermodynamic potential that indicates the direction of spontaneous processes and especially chemical reactions; in equilibrium, G assumes a minimum value. The Gibbs energy often takes the form of a Legendre transformation of the enthalpy, H, and the entropy, S, at the temperature T [Eq. (1)]

$$G = H - TS \tag{1}$$

but the notation of G in the form of the so-called Maxwell relations is entirely equivalent and likewise very common [Eq. (2)].

$$\mathrm{d}G = V\,\mathrm{d}p - S\,\mathrm{d}T \tag{2}$$

Upon the inclusion of pressure, p, and volume, V, as well as the internal energy, U, and the Helmholtz energy, A (sometimes also denoted as F, the thermodynamic potential for constant volume), all conceivable Maxwell relations can be easily written in the practical scheme by Guggenheim (see Figure 1).[13] If the energy of a system depends additionally on external fields (electric, electrochemical, magnetic, etc.), G is naturally extended accordingly.

Figure 1. Guggenheim scheme for quickly setting up the Maxwell relations between the thermodynamic potentials; the letter order can be remembered with the mnemonic "Good Physicists Have Studied Under Very Active Teachers."

In the digital age, the numerical description of a thermodynamic system of any number of chemically pure components now boils down to determining the smallest value of the Gibbs energy with the knowledge of every single potential and the help of a so-called "G minimizer";[11] a purely arithmetic problem for the fastest possible computers. For practical reasons, an enthalpy, H, and an entropy, S, for each

Ralf Peter Stoffel, born 1975 in Stolberg (Rhineland), studied chemistry at RWTH Aachen University and received his diploma in 2007 with an analysis of linear-scaling electronic-structure methods. He is currently working on his PhD in Richard Dronskowski's group. His research concerns parameter-free calculations of thermodynamic potentials of solid-state materials using quantum-chemical principles.

Claudia Wessel, born 1983 in Viersen, studied chemistry at RWTH Aachen University. For her diploma thesis she carried out quantum-chemical investigations of oxygen-conducting membranes. Since 2008 she has been working on her doctorate under the guidance of Richard Dronskowski. Her research is targeted at theoretical studies of metastable oxides and oxynitrides of the vanadium and chromium groups.

Marck Lumey, born 1974 in Heerlen (The Netherlands), studied chemistry at RWTH Aachen University and received his PhD with Richard Dronskowski in 2006. After a two-year postdoctoral stay in Aachen's Chemical Engineering Institute, he returned to the Chair of Solid-State and Quantum Chemistry in 2008. Since then, he has been specializing in performing quantum-chemical calculations on complex ion-conducting materials.

Richard Dronskowski, born 1961 in Brilon, studied chemistry and physics in Münster and received his doctorate under the guidance of Arndt Simon in Stuttgart in 1990. After a one-year stay as a scientific visitor with Roald Hoffmann, he completed his habilitation in Dortmund in 1995. In 1996 he accepted the offer of RWTH Aachen University where he currently holds the Chair of Solid-State and Quantum Chemistry. His interests lie in synthetic solid-state chemistry (carbodiimides, nitrides, intermetallic phases, metastable solids, structural research) and in the quantum chemistry of the solid state (electronic structure, magnetism, linear methods, phase prediction, thermochemistry).

substance are stored as a sum of a reference term (at standard conditions) and a temperature-dependent term, accordingly [Eq. (3)]

$$H = H^{\mathrm{ref}} + \int_{T_{\mathrm{ref}}}^{T} C_p \mathrm{d}T \;\text{ and }\; S = S^{\mathrm{ref}} + \int_{T_{\mathrm{ref}}}^{T} \frac{C_p}{T} \mathrm{d}T \tag{3}$$

so that the Gibbs energy can subsequently be put together mathematically according to the Gibbs–Helmholtz equation [Eq. (1)]. While at standard conditions, the value of H^{ref} of elements in their stable allotropes is set to zero by definition, and the measured values of S^{ref} are conveniently tabulated, the temperature-dependent heat capacity is expressed according to a suggestion from Meyer and Kelley[14] as a polynomial sum [Eq. (4)].

$$C_p = c_1 + c_2 T + c_3 T^2 + \frac{c_4}{T^2} \tag{4}$$

Finally from enthalpy, entropy, and the temperature-dependent heat capacity the expression for the Gibbs energy is obtained, which also can be formulated in the form of a polynomial expression [Eq. (5)].

$$G = A_1 + A_2 T + A_3 T \ln T + A_4 T^2 + A_5 T^3 + \frac{A_6}{T} \tag{5}$$

Conveniently, the coefficients A_i are stored in the so-called G databases. Without a doubt, this digitized information belongs to the most precious treasures of our technological civilization, and they are diligently cultivated and continuously expanded by their users, for example SGTE (Scientific Group Thermodata Europe), a combination of European and North-American research organizations. In cooperation with powerful classical software—such as ChemSheet, DICTRA, FactSage, GEMINI, Thermo-Calc, and others—they form the complete backbone for industries involved with thermochemical issues (energy production, chemistry, steel, etc.) and of course also for basic research[11] but this does not seem to be sufficiently known outside some disciplines.

The involuntary "blemish" of the above approach, however, exists in that the thermochemical databases for as yet unknown materials show absolutely no entry; unknown materials have simply not been measured yet. Similarly, there are "blank spots" for well-known materials in the databases, just because not every substance has been thermochemically measured under all possible conditions. Clearly table salt is an everyday substance, but which value, for example, does its entropy have at 73 K and a pressure of 145 GPa? Even if this value exists, how would it look after a compression of a further 20 GPa? We do not know, or at least not exactly, because the measurement has never been carried out.

The maturity of the ab initio electronic-structure theory, however, allows access to these data, namely through abandonment of the measurement and returning to the Schrödinger equation. By doing so, an enormous expansion of the thermochemistry can be achieved with respect to still completely unknown chemical systems and likewise nearly or completely inaccessible conditions. The key is found in the computational treatment of the temperature-dependent heat capacity that almost fully goes back to atomic movements, and it will be addressed below.

2.2. Temperature Dependence of Heat Capacity

The theoretically skilled probably recognize intuitively that the first-principles calculation of thermochemical state functions for finite temperatures should represent an enormous computational challenge. Nonetheless, even a cursory initial look shows that the energetic aspects allow a clear separation between nuclear and electronic dynamics. Temperature changes affect the nuclear motions almost exclusively, and not the electronic structure because electronic energies (electron volt; $1\,\mathrm{eV} \mathrel{\hat{=}} 11\,606$ Kelvin) are extremely large when compared with thermal ones (Kelvin; $300\,\mathrm{K} \mathrel{\hat{=}} 26\,\mathrm{meV} \mathrel{\hat{=}} 2.5\,\mathrm{kJ\,mol^{-1}}$); the ratio is about two orders of magnitude. Even for red- or white-hot solids, the electrons are still situated in the electronic ground state despite the vigorously vibrating atomic cores, so that the usual quantum-chemical computations can be adopted almost unchanged, if small correction terms are disregarded (especially important for metals, see Section 5). It is exactly these fortunate connections that made a first and rough estimate of the heat capacity of solids possible even before the discovery of quantum mechanics:

According to Dulong and Petit,[15] all atoms in a crystalline solid vibrate at room temperature in all three dimensions with an energy of $k_{\mathrm{B}} T$, so that for the internal energy, U, for a mole of a crystal made of one atom type, Equation (6) applies.

$$U = 3 N_A k_{\mathrm{B}} T = 3 R T \;\text{ and }\; C_V = \left(\frac{\partial U}{\partial T}\right)_V = 3R \approx 25\,\mathrm{J\,K^{-1}\,mol^{-1}} \tag{6}$$

Indeed, very many experimental heat capacities at constant volume actually lie in the order of magnitude of this $25\,\mathrm{J\,K^{-1}\,mol^{-1}}$, however, C_V drops off to zero fairly quickly for decreasing temperatures. This quantum-mechanical effect was already described qualitatively and correctly by Einstein,[16] and indeed with the more or less plausible assumption that all atoms vibrate with the same frequency, ω_E, and the energies of these vibrations are quantized according to $E = n\hbar\omega_E$. Thus Equation (7) is obtained for the internal energy:

$$U^E = \frac{3 N_A \hbar \omega_E}{e^{\hbar\omega_E / k_{\mathrm{B}} T} - 1} \tag{7}$$

and accordingly for the heat capacity [Eq. (8)]

$$C_V^E = 3R\xi \;\text{ where }\; \xi = 3\left(\frac{\theta_E}{T}\right)^2 \left(\frac{e^{\theta_E/2T}}{e^{\theta_E/T} - 1}\right)^2 \tag{8}$$

and the so-called Einstein temperature $\theta_E = \hbar\omega_E / k_{\mathrm{B}}$.

A plot of Einstein's heat capacity for elemental copper with a face-centered cubic structure is shown in Figure 2. For high temperatures ($T \gg \theta_E$) a series expansion results immediately in the Dulong–Petit value of $3R$, and for low temperatures an exponential decay is found, accordingly [Eq. (9)]

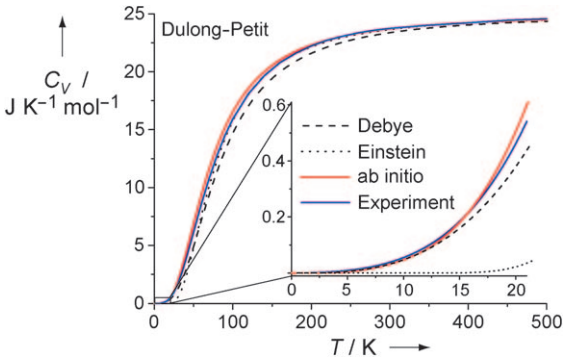

Figure 2. Density-functional-theory-calculated (plane waves, pseudopotentials, GGA) heat capacity of face-centered cubic copper at constant volume (red) as a function of temperature, with experimental values from ref. [17,18] (blue) as well as the Debye (dashed) and Einstein (dotted) models for comparison.

$$\xi \approx \left(\frac{\theta_E}{T}\right)^2 \left(\frac{e^{\theta_E/2T}}{e^{\theta_E/T}}\right)^2 = \left(\frac{\theta_E}{T}\right)^2 e^{-\theta_E/T} \qquad (9)$$

which differs significantly from the actual trend.[19]

Debye finally recognized[20] that, in solids, not all vibrations exhibit the same frequency. For quantitative calculations it is much more essential to find the density of states for all vibrational states. The Debye theory, which is discussed in many famous physical chemistry textbooks,[21,22] gives, then, for the heat capacity at constant volume [Eq. (10)]

$$C_V^D = 3R\xi \text{ with } \xi = 3\left(\frac{T}{\theta_D}\right)^3 \int_0^{\frac{\theta_D}{T}} \frac{x^4 e^x}{(e^x-1)^2}\,dx \qquad (10)$$

with the so-called Debye temperature $\theta_D = \hbar\omega_D/k_B$.

This approximation for C_V is also plotted in Figure 2, and it delivers the actual trend of the heat capacity at low temperatures (T^3 law[19]) semi-quantitatively correct because near absolute zero only long-wave vibrations of low energy are active. Nonetheless, the Debye approach is built upon a completely unstructured, exemplary density of states that increases simply with the square of the vibrational frequency, and this approximation does not apply in general. Figure 3 shows a schematic comparison of these densities of the vibrational states from the Einstein and Debye models, as well as, for comparison, a modern quantitative calculation based on a quantum-mechanical treatment. To be able to calculate a realistic heat capacity that differs from substance to substance,[23] the explicit compilation of all vibrational states using quantitative theoretical techniques across the models of Einstein and Debye is necessary.

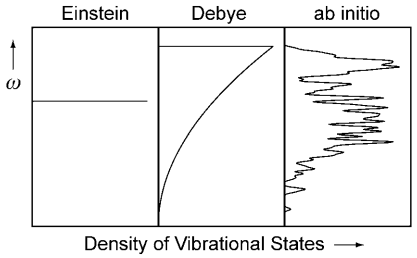

Figure 3. Frequency distribution of the vibrational states of face-centered cubic copper according to the Einstein and Debye models, as well as on the basis of first-principles density-functional calculations.

If such a first-principles (and not exemplary) calculation of the vibrational states succeeds, then the quantum-chemically calculated and experimentally measured heat capacities run practically congruent, and this over the whole temperature range; this is also shown in Figure 2 for the admittedly very simple case of face-centered cubic copper. In order to cover these atomic displacements correctly, additional considerations are necessary, which will be discussed at length in the next sections.

3. Temperature-Dependent Atomic Displacements

Despite the fundamental translationally invariant structure of crystalline solids, one always faces two borderline cases for physicochemical properties in condensed matter, in fact independent of whether or not they touch upon the ground state or different excited states. As is well known, a magnetic property can result, for example, from a local magnetic moment of a single atom incorporated in a lattice, but delocalized magnetic properties like itinerant ferro-, antiferro-, and ferrimagnetism often exist.[24] Likewise, an optical signal may originate from the electronic excitation of a single atom in a solid, such as with 4f atom-doped phosphors,[25] but the excitations could of course also be thought of in the form of a collective or even coherent state that sweeps over the whole crystal, as in the classic case of the ruby laser.[26] And, naturally, the antagonism of localization and delocalization is also found for atomic excitations which, therefore, lends itself to a simplified breakdown for better overview.

3.1. Local Excitations

The calculation of local excitations of atoms, ions, or entire molecules has—because of the existence of transition states—an outstanding meaning in chemistry, and the more so, the more "kinetic" the underlying chemical problem is. In this context we are reminded, for example, of the investigation of catalytic processes on surfaces[27] or of atomic-diffusion processes in solids,[28] which will play a weighty role in this Review. As is generally known, with increasing temperature defects are necessarily produced in every crystalline solid, for reasons of entropy, and single atoms begin to migrate between

alternative atomic positions as a function of the available energy. Fortunately, quantum-chemical methods these days are in the position to determine the sought-after transition states or reaction pathways, though with differing certainty. If the reaction pathway is clarified with atomic resolution, the chemical processes may also be understood and possibly optimized.

Meanwhile, various theoretical strategies exist to calculate local excitations,[29] but herein, for reasons of conciseness, we want to concentrate on a particularly successful method, namely that of the "nudged elastic band," NEB.[30] The reader is also referred to alternative methods for the sampling of the energy hypersurface, such as meta-dynamics,[31] parallel tempering,[32] or transition-path sampling.[33]

Insofar as the activation energy for the diffusion process of a single atom needs to be theoretically identified, the minimum-energy path for this diffusion process must be found, and it must, therefore, be concerned with the reaction pathway that connects the beginning and ending states by the lowest energy. In other words, the educt state, the product state, and the transition state of a reaction process lie on specific points on the same hypersurface of the potential energy, and all three can be dealt with by electronic-structure calculations, though in a different form: the thermodynamically stable beginning and ending states correspond to the (absolute or regional) minima of the hypersurface, and reactive intermediates are identified as local minima. Therefore the reaction rate-determining transition state is a first-order saddle point on the hypersurface (see Figure 4).

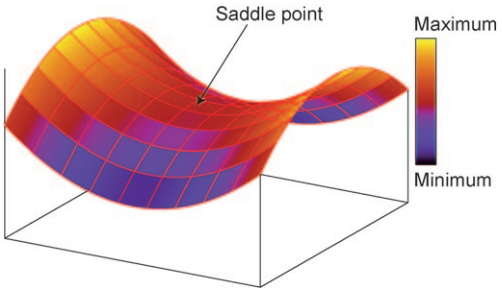

Figure 4. Schematic representation of a hypersurface of the potential energy with two minima, two maxima, and a first-order saddle point.

A first-order saddle point is a maximum in one direction and a minimum in all other directions, so that for the calculation of the transition state a method that guarantees the maximization of one degree of freedom and the simultaneous minimization of all others must be used; it is this that makes NEB the method of choice because it is very efficient at finding the minimum energy path between the beginning and ending states. For example, to calculate the reaction pathway of a diffusion process, a series of geometric "images" between the (more or less stable) beginning and ending states are produced, which usually differ only with respect to the position of the migrating atom. The structural optimizations of every single intermediate image based on the Schrödinger equation, however, are not totally independent of each other, but they are rather connected with the help of an artificially introduced interaction ("spring") between the images. In this way, a sort of "elastic band" is imitated, which is schematically illustrated in Figure 5. Now for the energetic optimization of the band all of the acting forces in the individual transition steps ("images") are systematically minimized, so that the

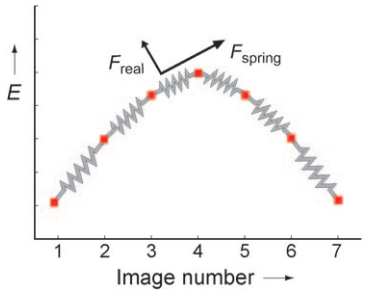

Figure 5. Schematic representation of the intermediate steps coupled by "springs," as well as the breakdown of the forces into the force, F_{real}, acting perpendicular to the elastic band, and the parallel spring force, F_{spring}.

band finally describes the minimum-energy pathway. The necessity of such a seemingly random elastic band is immediately apparent because a conventional optimization of a transition state leads to a relaxation either into the beginning or ending state.

The NEB method is particularly characterized by its force projection. It guarantees that the artificial spring forces between the images will not be disturbed by the optimization of the band and that the arrangement of the intermediate steps along the path remains uninfluenced. This continuous independence of the spring forces from the minimum-energy path is reached in the following way: for every optimization at each intermediate step a tangent is created to the band, which allows a partitioning of the forces acting on the intermediate images (see Figure 5). Parallel to the tangent is the spring force, which controls the distance between the images, and perpendicular to that is the actual potential force, which needs to be minimized. The total force, which acts on an intermediate image, is composed of the sum of the spring force along the tangent and the potential force perpendicular to it.

3.2. Collective Excitations: Phonons

The atoms present in crystals experience different collective or lattice vibrations under thermal excitation. As a result of the quantum-mechanical laws, the energies of the lattice vibrations are quantized according to Equation (11)

$$E_n = (n + {}^1/_2)\hbar\omega \qquad (11)$$

and the zero-point energy, ${}^1/_2\hbar\omega$, is invariably present, even at absolute zero. The corresponding quasiparticle belonging to the collective vibration is called a phonon in physics. The propagation of a phonon occurs along the wavevector **k** with the value $k = 2\pi/\lambda$, where λ stands for the wavelength of a phonon.

In full analogy to the case of extended electronic states—the so-called electronic "band structure"[34]—the translational invariance of a solid enforces a pronounced dispersion relation for the phonon energies, which can be understood easiest for model systems for which they yield the so-called phonon band structure. We imagine a one-dimensional and infinitely long chain of hydrogen atoms—the Drosophila of solid-state quantum chemistry—which, as a function of its chemical bonding and the underlying electronic structure, is again bound together by a "spring" with the spring constant f; this model is shown schematically in Figure 6 (top). Naturally the "spring" reflects the sum of all the quantum-chemical bonding forces.

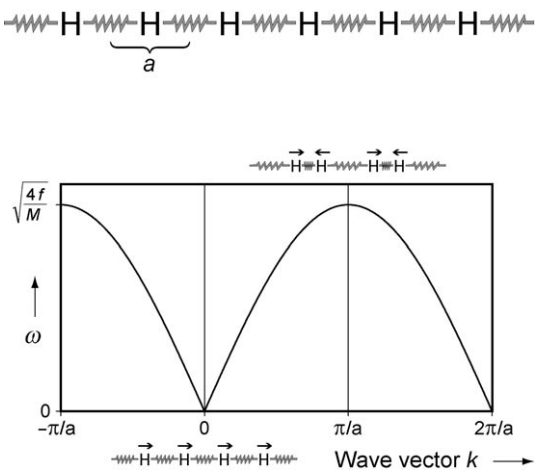

Figure 6. Top: one-dimensional infinite chain of hydrogen atoms with the equilibrium distance a; the atoms are connected by a "spring", which symbolizes the sum of the chemical bonding forces. Bottom: analytical phonon dispersion of this one-dimensional infinite chain of hydrogen atoms with the atomic mass M.

Employing one hydrogen atom per unit cell with the lattice parameter a, produces the worked example found in all basic textbooks of solid-state physics.[35,36] The analytical calculation also yields a phonon frequency, ω, which is dependent on the wave vector, k, and the atomic mass, M [Eq. (12)]

$$\omega = \sqrt{\frac{4f}{M}}\left|\sin\frac{1}{2}ka\right| \tag{12}$$

and plotting ω as a function of k provides the phonon band structure shown in Figure 6 (bottom). As a consequence of the one-dimensional problem, we have dispensed with the vector notation in favor of readability.

At the zone center, Γ ($k=0$), an H atom is in phase with all neighboring atoms, so that the H–H distance is constantly a; no spring is compressed or stretched, and the frequency, and with it the energy, is equal to zero; the whole H chain in Figure 6 (top) moves in concert in one direction. For small wave vectors, k, the frequency, ω, increases almost linearly and begins to deviate noticeably from the linear path only close to the zone edge, X ($k=\pi/a$), and it meets the X point horizontally. Precisely at this point the phonon velocity, $v = \mathrm{d}\omega/\mathrm{d}k$, is exactly zero, so that a "standing" wave with the frequency $\sqrt{4f/M}$ is found. For an analogous one-dimensional chain of lithium atoms with the same spring constant for the Li–Li bond, the frequency would be smaller by a factor of $\sqrt{7}$, the square root of the ratio of the atomic masses of Li to H. In a complete analogy to electronic band structures, the phonon band structure exhibits a periodicity of $2\pi/a$, so that it is absolutely sufficient to remain in the region of only the first Brillouin zone.[37,38]

The phonon band structure of a one-dimensional chain of Li and H atoms with equidistant Li–H distances is only slightly more complicated. The lattice parameter a still describes a one-dimensional unit cell that now contains two atoms (see Figure 7, top), and necessarily two branches are found in the phonon band structure (Figure 7, bottom).

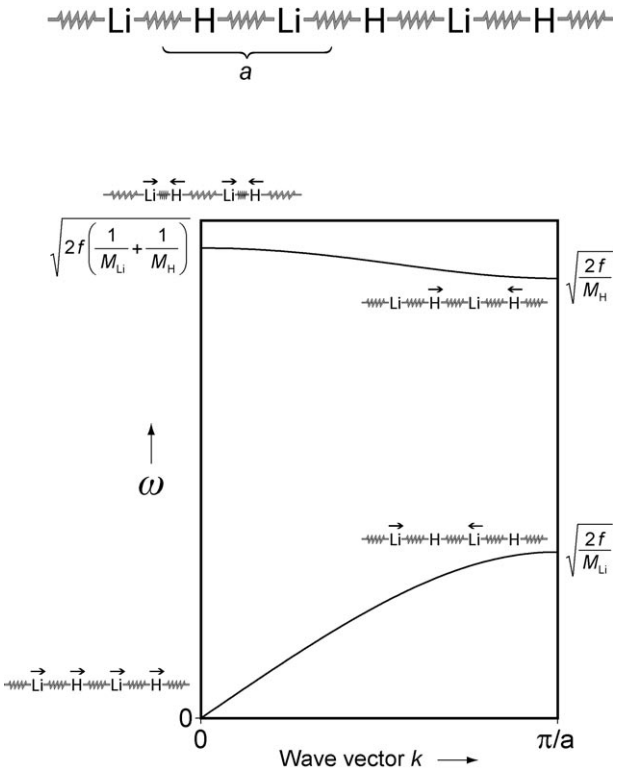

Figure 7. Top: one-dimensional infinite chain of lithium hydride with the equilibrium distance a; the atoms are connected by a "spring", which symbolizes the sum of the chemical bonding forces. Bottom: analytical phonon dispersion of this one-dimensional infinite chain of LiH with the atomic masses M_{Li} for lithium und M_H for hydrogen.

The energies of both branches are analytically easy to specify;[35,36] for a Li–H spring constant, f, the calculation of the frequency arrives at [Eq. (13)]

$$\omega = \sqrt{f\left(\frac{1}{M_{Li}}+\frac{1}{M_H}\right) \pm f\sqrt{\left(\frac{1}{M_{Li}}+\frac{1}{M_H}\right)^2 - \frac{4}{M_{Li}M_H}\sin^2\frac{ka}{2}}} \tag{13}$$

so that the phonon frequencies at the zone center and edge, inserted in Figure 7 (bottom), are produced through a simple

substitution ($k = 0$ and π/a). The lower branch of the phonon band structure disappears because $\omega = 0$ in the zone center, Γ, and is called the "acoustic" branch; the upper branch (with $\omega(\Gamma) \neq 0$) is called the "optical" branch because it can be coupled to a photon (e.g., infrared radiation) if there is an interatomic charge-transfer and, therefore, a resulting dipole moment. The high energy of the optical branch at Γ stems from the fact that, although the displacements in each unit cell are in phase, Li and H vibrate against each other with an average mass. At the zone edge, X, on the other hand, vibrational modes have very different characters, and indeed either the heavy (Li, acoustic branch, Figure 7, bottom, lower trace) or the light (H, optical branch, Figure 7, bottom, upper trace) atomic lattice vibrates there, and, therefore, only the Li or the H atomic mass appears in the frequency. The other atomic lattice rests. The generalization for the case of three-dimensional systems has been known for a long time.[39] If a unit cell contains N atoms, the phonon band structure exhibits exactly 3 acoustic and $3N-3$ optical phonon branches.

Now let us consider a simple three-dimensional example, namely face-centered cubic copper (fcc-Cu), whose primitive cell contains only one Cu atom. Its phonon band structure, shown in Figure 8, can only exhibit acoustic branches, of

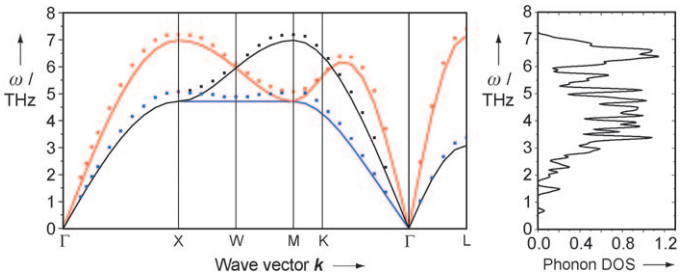

Figure 8. Density-functional-theory-calculated phonon dispersion (left) and phonon density of states (right) of face-centered cubic copper; theoretical values: solid lines; experimentally measured values: dots.

which one is "longitudinal" in nature because the direction of vibration coincides with the direction of propagation, totally analogous to the symmetry of the σ-interaction in electronic systems. In addition, there are two "transversal" branches for fcc-Cu, in which the vibration runs perpendicular to the direction of propagation, and this resembles the symmetry of the π-interaction. Diamond, with two atoms in the unit cell ($N = 2$), logically has a phonon band structure with 3 acoustic and 3 optical branches; even when, as a result of the missing dipole moment on the optical branches, it cannot be IR-spectroscopically coupled, nothing in the naming is changed.

To better understand the phonon band structure of copper, the corresponding Brillouin zone of the primitive unit cell of the face-centered cubic structure, as well as the vibrational modes[39] at points $\mathbf{k} = (2\pi/a)(1,0,0)$ (**X** point) and $\mathbf{k} = (2\pi/a)(1/2,1/2,0)$ are shown in Figure 9. At **X**, the wave vector, **k**, points in the x-direction, and the wavelength is $\lambda = a$. Neighboring atomic planes vibrate against each other and necessitate the energetic degeneration of both transversal

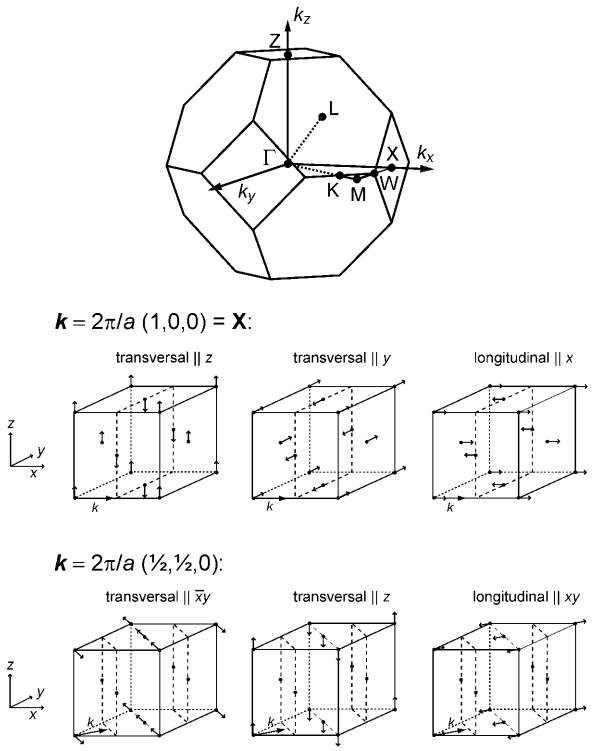

Figure 9. First Brillouin zone (top) of a face-centered cubic unit cell[40,41] indicating the special k-points and the schematic representations of the phonons of this unit cell (bottom) at two chosen special points; they can be compared with the phonon dispersion of face-centered cubic Cu from Figure 8.

modes. In the longitudinal mode, the atoms vibrate against each other but in the direction of the next atom, so that at equal vibrational amplitudes a larger compression and stretching of the interatomic bonds results. Therefore, the frequency of these vibrations is higher than both the others.

The vibrational modes at point $\mathbf{k} = (2\pi/a)(1/2,1/2,0)$, at the halfway to point **M**, so to speak, are each energetically different. The direction of propagation at this point is the diagonal of the xy-plane, and the wavelength is $\lambda = \sqrt{2}a$, so that every second atomic plane is at rest, while the other planes vibrate against each other. At the **M** point, $\mathbf{k} = (2\pi/a)(1,1,0)$, not shown here, the wavelength is $\lambda = a/\sqrt{2}$, and the propagation direction is also the diagonal of the xy-plane. The **M** point is not, however, situated in the original Brillouin zone, rather it is equivalent to the **Z** point, $\mathbf{k} = (2\pi/a)(0,0,1)$, of another Brillouin zone. Therefore, it is possible to think of the vibrational states at the **M** point as being like those at the **X** point, though with the direction of propagation of the plane wave parallel to z.

Through summation over all phonon frequencies, ω, occurring in reciprocal space, a phonon density of states, pDOS, can of course be calculated, which can be conveniently plotted side-by-side with the phonon band structure (Figure 8). The pDOS brings us significantly closer to the total vibrational energy of the crystal (see Section 3.3). In the three-dimensional case, the phonon density of states is obtained from [Eq. (14)]

$$\mathrm{pDOS}(\omega) = \sum_j g_j(\omega) \;\text{ with }\; g_j = \frac{Na}{\pi}\frac{\mathrm{d}\mathbf{k}}{\mathrm{d}\omega} \tag{14}$$

in which the phonon dispersion is integrated over all branches, j. Exactly as in the "electronic" case,[37,38] a high dispersion is linked with a low density of states and vice versa.

In consideration of the symmetry analysis along special points in the first Brillouin zone, the three-dimensional phonon band structure of fcc-Cu shown in Figure 8 is consequently understandable in the smallest detail. Additionally, Figure 8 provides not only the ab initio calculated values (solid line), but also those frequencies taken from experimental measurements (dotted), for example, from inelastic neutron scattering. Already the name of the latter technique indicates it is an energy-loss spectroscopy using a particle beam.[35,36] For the determination of the phonon dispersion the momentum theorem is [Eq. (15)]

$$\mathbf{k} + \mathbf{G} = \mathbf{k}' + \mathbf{K} \tag{15}$$

and in this case $\mathbf{k}$ and $\mathbf{k}'$ are the scattering vectors of the incident and scattered (emitted) neutrons, $\mathbf{G}$ is an arbitrary reciprocal lattice vector, and $\mathbf{K}$ is the created (or annihilated) phonon. At the same time, the energy theorem [Eq. (16)]

$$\frac{\hbar^2\mathbf{k}^2}{2M_n} = \frac{\hbar^2\mathbf{k}'^2}{2M_n} \pm \hbar\omega \tag{16}$$

must be fulfilled so that only the neutron energy needs to be investigated as a function of the scattering angle. This is certainly a mature method in solid-state physics, yet to this day we know the actual phonon dispersions of very few very simple materials, simply due to the extreme experimental complexity: angle-resolved neutron spectroscopic experiments of large single crystals are difficult to apply for and, if permitted, are no less difficult to carry out and evaluate.

3.3. Free Phonon Energy

Apparently the exact knowledge of the vibrational states of a solid is the key to the calculation of its thermodynamic properties as a function of temperature. Once the electronic (ground) state of a system of nuclei and electrons is certain, this system must then only be "raised" to the desired temperature and have its free energy analyzed there.[42]

If we could know with absolute certainty the spring constant, f, of the one-dimensional H or Li–H chain mentioned already, for example, then a (microcanonical) ensemble of several thousand H or Li atoms in a given volume could be prepared, and its evolution[43] would be monitored over time in the context of molecular dynamics.[44,45] Alternately, all the nuclear configurations could be randomized according to the Monte Carlo procedure,[46] and the thermodynamic equilibrium ascertained in a purely stochastic way. Both procedures are quite plausible and computationally the last resort, and for that very reason a much simpler approach is apparent, which is positioned closer to the electronic-structure theory of solids:

Starting from the "spring" forces, we have already discussed the central meaning of the phonon frequency, ω. It is possible to calculate not only the phonon density of states from the frequencies, but also, and much more importantly, the so-called temperature-dependent harmonic phonon energy; it is simply given by Equation (17).

$$E_{\mathrm{ph}} = \sum_{\mathbf{k}} \hbar\omega(\mathbf{k})\left[\frac{1}{2} + \frac{1}{\exp(\hbar\omega(\mathbf{k})/k_{\mathrm{B}}T) - 1}\right] \tag{17}$$

For the sake of brevity, we will forgo the derivation,[35,36] but it should at least be mentioned that the above expression is based, on the one side, on the energy equation of the harmonic oscillator [Eq. (11)] and, on the other side, takes into account the fact that phonons, as boson quasiparticles, are subject to Bose–Einstein statistics. If the classical thermochemical expression for the heat capacity according to Equation (6) is used, the heat capacity at constant volume can be stated directly [Eq. (18)]:

$$C_V = \left(\frac{\partial U}{\partial T}\right)_V = \left(\frac{\partial\{U^{0\mathrm{K}}_{\mathrm{calculated}} + E_{\mathrm{ph}}\}}{\partial T}\right)_V = \left(\frac{\partial E_{\mathrm{ph}}}{\partial T}\right)_V \tag{18}$$

So we have assembled the internal energy, U, from a temperature-independent basis term at absolute zero and the temperature-dependent harmonic phonon energy, and because the first term does not depend on the temperature, it falls out of the differential equation. Now there is also a simple mathematical connection (see Appendix B) between the partition function, Z, and the harmonic phonon energy, so that the free phonon energy, A_{ph}, ultimately becomes [Eq. (19)].

$$A_{\mathrm{ph}} = \frac{1}{2}\sum_{\mathbf{k}} \hbar\omega(\mathbf{k}) + k_{\mathrm{B}}T\sum_{\mathbf{k}} \ln[1 - \exp(-\hbar\omega(\mathbf{k})/k_{\mathrm{B}}T)] \tag{19}$$

We arrive at the conceptually strikingly simple result that for the determination of the harmonic—and in computational practice actually quasiharmonic (see Section 4.2)—free vibrational energy dependent on the temperature, only the phonon frequencies are actually searched for, and these are directly calculable using quantum-mechanical measures. From the free vibrational energy the free enthalpy (or Gibbs energy) is reached relatively simply, and the free road to ab initio thermodynamic modeling is paved.

4. Principle Approach

4.1. Electronic Structure Theory

For the theoretical calculation of the electronic structure of condensed matter we search for the solution to the stationary wave equation by Schrödinger [Eq. (20)][47]

$$\mathscr{H}\Psi = E\Psi \tag{20}$$

or its relativistic formulation by Dirac,[48] in which the Hamilton operator, $\mathscr{H}$, through the use of the Born–

Oppenheimer approximation,[49] consists of only the kinetic energy of the electrons, their potential energy in the nuclear field, and the electron–electron interaction; the nuclei are at rest, and the electrons interact, first, with the atomic cores and, second, with each other, just as is known from molecular quantum chemistry.[50–54]

The difference from the molecular problems becomes apparent for crystalline materials on the basis of the translational invariance of the nuclear potential, which is taken into account by means of Bloch's theorem,[55] so that any linear combination of atomic orbitals (LCAO) does not lead to molecular, but rather to crystal orbitals, whose chemical (bonding) interpretation proceeds fully analogously to molecular quantum chemistry.[37] This very construction of the extended wave function from local functions seems rightly chemically transparent, and therefore there exist diverse, variably precise, and, as a rule, numerically sophisticated procedures[56–61] whose advantages and disadvantages are covered in corresponding textbooks.[38]

On the other hand, for periodic systems, the construction of the extended wave function from plane waves according to $\exp\{i\mathbf{kr}\}$ as a "natural" basis is fairly obvious,[38] and its size can be adjusted simply by means of an energetic cut-off criterion. Despite the chemical opaqueness, this approach exhibits enormous computational advantages (e.g., the disappearance of all Pulay forces[62]), however, it requires the use of pseudopotentials[63] so as not to have to take into account the high kinetic energy of the core electrons. In combination with highly efficient approaches to the generation of diverse pseudopotentials,[64–79] as well as all-electron-methods-based pseudopotential descendants (on the lines of projector-augmented wave, PAW[80]) is the triumph of the combination of pseudopotentials/plane waves impressive and, at the same time, easily understood.[81,82] Unproblematic to use, numerically reliable and, as a rule, stably operating computer programs such as VASP, CASTEP, ABINIT illustrate this fact. The complete equivalence of the "local" (atomic orbitals) and "delocalized" (plane waves) approach for the calculation of electronic structures has been recently and convincingly illustrated.[83]

The extent of the electron–electron interaction is usually taken into account by the methods of density-functional theory (DFT),[84–88] although the Hartree–Fock approximation[89,90] in combination with periodic approaches for the explicit inclusion of the electronic correlation[91] by Møller–Plesset[92] is currently undergoing a certain renaissance and probably will become even more important in the long run. Within DFT the local-density approximation (LDA)[88] takes a central role in various numerical parameterizations.[93–95] The generalized-gradient approximation (GGA), with a variety of parameterizations,[96,97] is credited with higher numerical accuracy, especially with regard to atomic energetics, although the results vary depending on the question.

With the inclusion of finite temperatures, however, it is possible (at least partially) to revise a prevalent prejudice.[38] It is often reported that the LDA, because of a certain energetic "overbinding", underestimates the lattice parameters of crystalline materials by several percent, whereas the GGA usually leads to a slight overestimate of the same lattice parameter. That is correct, however, for these comparisons almost always the lattice parameters at room temperature are used, and not those at absolute zero. In this way the lattice parameter of fcc-Cu at room temperature, for example, is exactly 3.615 Å, and the value calculated for absolute zero is 3.517 Å using the LDA (2.3% underestimate) and 3.644 Å using the GGA (0.8% overestimate).

We would like to consider a more extreme case, namely solid lithium hydride in the rock-salt structure. Figure 10 demonstrates that, on the basis of the pure electronic energies

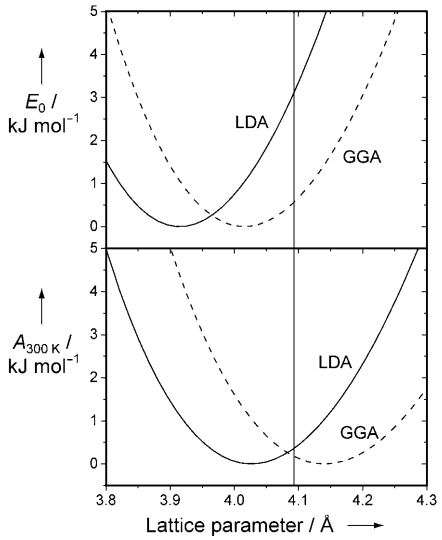

Figure 10. Density-functional-theory-calculated energy–volume curves for lithium hydride on the basis of the LDA (solid) and the GGA (dashed). In the upper part of the diagram, electronic total energies are presented, and in the lower part Helmholtz energies at 300 K are given. The experimental lattice parameter at 300 K (4.093 Å) is marked as a vertical line.

(Figure 10, top), that the LDA very plainly (4.4%) underestimates the lattice parameter of LiH at room temperature, and even the GGA leads to a distinct underestimate (1.9%), and not to an overestimate. The plot of the Helmholtz energy (Figure 10, bottom) shows that the influence of the zero-point vibration and the lattice vibrations excited at 300 K lead to a significant lattice expansion, for both the LDA, as well as for the GGA. Whether at room temperature the LDA (about 1.6% too small) or the GGA (about 1.2% too large) is the more convincingly powerful description may be argued, in truly good agreement with independent observations.[98]

Granted, LiH is an extreme case because for such light atoms, the zero-point vibration carries enormous weight. The successive widening of the lattice parameters, and therefore the diminution of the density, can also be demonstrated in fcc-Cu. A comparison of the density's temperature-dependency is depicted in Figure 11, and in fact based on both LDA and GGA functionals. Compared with the experimental values,[99] the supposed overestimate (LDA) and underestimate (GGA) are apparent, and indeed over the entire temperature range up to the melting point of 1358 K.

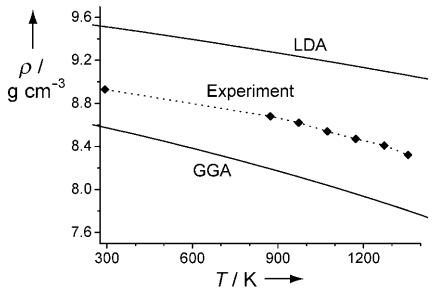

Figure 11. Density-functional-theory-calculated density of copper on the basis of the LDA and the GGA (both solid lines). The experimental density (diamonds and dashed line) lies between the two theoretical values.

From the aforementioned explanations of electronic-structure theory, a sort of "complementary relationship" between experiment and theory with respect to the thermodynamic treatment of solids may be recognized: While the exertion of high pressures (somewhere in the gigapascal region) is connected to greatest efforts and enormous costs (high-pressure instruments) for the experimenter, the theoretical description costs the theoretician only a small shrug of the shoulders because only the interatomic distances (or the lattice parameters) are contracted for the self-consistent solution of the Schrödinger equation, thus a trivial modification of the problem. On the other hand, the temperature, which constitutes the experimentally simplest to set and "cheapest" state value (Bunsen burner, heating coil, cold trap, etc.), makes the theoretician sweat in the truest sense of the word. If it is a matter of a local thermal excitation, "only" a single atom is dislocated, and this is synonymous with the breaking of translational symmetry, which is always bought with an increased computational effort, especially when it concerns the step-wise calculation of an activation energy; the introduction of supercells is no exception. For collective excitations in the form of lattice vibrations (phonons) the computational effort rises immensely at the same time owing to the absolutely necessary supercells, because the required calculation time grows roughly proportional to the third power of the system's size; a hundred- to thousand-fold (!) increase in computational power is required, though it is still smaller than with molecular dynamics or the Monte Carlo approach.

4.2. Calculation of Phonon Frequencies

An extremely straightforward way to calculate phonon frequencies based on first-principles electronic-structure methods of periodic systems is given by the so-called *Direct Method*.[100,101] To this end, individual atoms of a preliminary translationally invariant lattice are dislocated just a little, such that the resulting perturbed system is treated the same way in terms of electronic-structure theory as the unperturbed system. The changed phonon frequencies or energies thus exactly reflect the geometric differences between the systems.

Now the desired frequencies are determined in that the energies of the different vibrational states are calculated with different wave vectors, **k**, as "snapshots" of the atomic displacements; the so-called "frozen phonon" method is defined this way. However, this approach remains limited to certain wave vectors, namely those that correspond to the supercell chosen by calculation, that is, those that geometrically fit inside it. For the calculation of the phonon dispersion over the entire Brillouin zone, the following approach is much more appropriate, which is targeted, in the first step, at the calculation of the ab initio force constants.

Assuming the simplifications as before, namely that the vibrations in solids are, to a first approximation, those of harmonic oscillators, it is possible to construct, analogous to the force constant, f, of the diatomic harmonic oscillator [Eq. (21)]

$$F = -f\,x \;\text{ or }\; f = -\frac{F}{x} \tag{21}$$

a so-called force-constant matrix [Eq. (22)]

$$\Phi_{\alpha\beta} = -\frac{F_\alpha}{d_\beta} \tag{22}$$

where F_α is the force acting upon an atom in direction α, provided another atom is moved by d along direction β. α and β stand for one of the Cartesian directions x, y, or z. Considering the crystalline symmetry simplifies part of the problem, sometimes enormously, just because only the symmetry-inequivalent atoms and directions must be taken into account and, therefore, the calculation of many force constants may be entirely dropped. The single force, provided electronic self-consistency according to the theorem by Hellmann and Feynman [Eq. (23)],[102,103]

$$\mathbf{F} = -\frac{\mathrm{d}E}{\mathrm{d}\mathbf{R}} = -\left\langle \Psi \left| \frac{\partial \mathscr{H}}{\partial \mathbf{R}} \right| \Psi \right\rangle \tag{23}$$

read so that the procedure, despite the harmonic approximation (oscillator approach), is revalued to the quasiharmonic approximation arising from the correctly calculated force for the exact potential, a severely under-appreciated advantage.

We would like to elucidate this lucky circumstance somewhat further, namely on the basis of Figure 12, which shows the calculated potential energy of face-centered cubic copper by ab initio electronic-structure theory. Near the

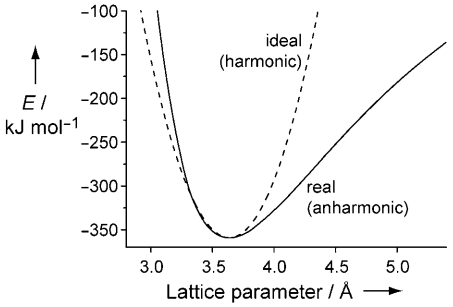

Figure 12. Density-functional-theory-calculated potential energy of face-centered cubic copper (solid) and its harmonic approximation (dashed) around the equilibrium volume.

equilibrium volume, that is, at the lowest point of the energy curve, the actual potential and its harmonic approximation (Figure 12, dashed line) run nearly congruent, and the above-mentioned idea of (harmonic) force constants [Eq. (21)], as well as all further computational steps, works for this reason only. If, however, we compress the solid very strongly together or overstretch the interatomic distances into the clearly anharmonic region, the accurate electronic-structure theory of the real, anharmonic potentials ensures that this anharmonicity implicitly flows into the still harmonically approximated phonons, that is, in the form of the aforementioned quasiharmonicity.

Once all the interatomic forces are calculated, the force-constant matrix is finally transferred, using a Fourier transformation, in the so-called dynamical matrix, D (see Appendix B), so that finally the determinant can be set equal to zero, and thus provides the desired phonon frequencies in one step (see Appendix B). In that respect this sort of lattice dynamics quite naturally couples with the common apparatus of electronic-structure theory for solids and trades the numerical calculation of the interatomic forces with the assembly of supercells (see Section 5) because the assumed fast decay of the forces is correct. The alternative approach of linear-response theory—based on the perturbation theory formulation of density-functional theory—operates, instead, with the un-enlarged unit cell and accesses the dynamical matrix at many wave vectors.[42,104]

5. Practical Implementation

Within our chosen approach, the quantum-chemical total energies of solids are obtained fundamentally for a constant volume (in computational practice, therefore, a constant volume of the unit cell), and for this reason it is only logical to calculate the desired pressure-dependent Gibbs energy, $G(p,T)$, based on the volume-dependent Helmholtz energy, $A(V,T)$ [Eq. (24)].

$$G(p,T) = A(V,T) + pV = A(V,T) - \left(\frac{\partial A}{\partial V}\right)_T V \tag{24}$$

The clever stroke is to determine the pressure from the negative change in the Helmholtz energy with respect to the volume, which arises from the collective displacements of all the atoms. In practice, the Helmholtz energy is calculated for this purpose at different volumes, and the resulting values are fitted, for the respective temperatures, by a simplified equation of state (EOS), for example, that of Murnaghan[105] or of Birch,[106] which we explore in detail in Appendix B. The Helmholtz energy, in turn, consists of several terms [Eq. (25)]

$$\begin{aligned} A(V,T) = {} & E_0(V) + A_{\mathrm{ph}}(V,T) + \Delta A_{\mathrm{el}}(V,T) + \\ & A_{\mathrm{conf}}(T) + A_{\mathrm{vib}}^{\mathrm{ah}}(V,T) \end{aligned} \tag{25}$$

where E_0 is the energy of the electronic ground state and A_{ph} is the so-called free harmonic vibrational energy [Eq. (19)]. Certainly, we must take into account even smaller additional temperature-dependent terms to achieve greater accuracy, thus initially the free electronic energy based on electronic excitations (relevant for systems with small or vanishing electronic band gaps), noted herein as ΔA_{el}, which, in combination with E_0, defines the total free electronic energy, A_{el}. To this is added a configurational term, in the case of systems with statistical occupations ($A_{\mathrm{conf}} = G_{\mathrm{conf}} = -TS_{\mathrm{conf}}$, since this term is naturally volume independent), as well as that part of the vibrational energy which can be traced back to anharmonic effects. Indeed, these anharmonic effects first appear in the heat conduction of real substances but this part of the computation is by far the hardest to overcome. As has already been explained, its explicit consideration, when the system is far enough from the melting point, can fortunately be ignored to a very good approximation, especially since the inclusion of the actual potential (see previous explanation) is equivalent to the quasiharmonic approximation and therefore implicitly includes a significant part of the anharmonic share. In this case nature turns out to be rather kind to the theoretician.

As an illustration, we show in Figure 13 the trend of the volume-dependent Helmholtz energy of barium oxide, BaO, at different temperatures. Initially the Helmholtz energy, with

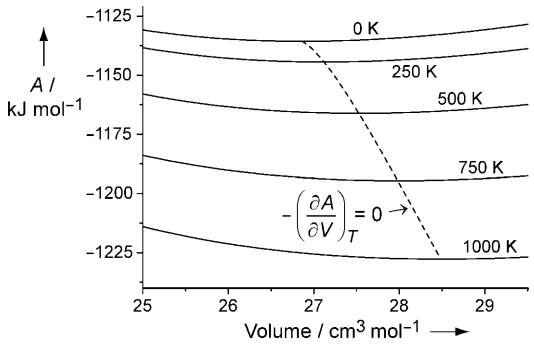

Figure 13. Density-functional-theory-calculated trend of the Helmholtz energy, *A*, for barium oxide as a function of the volume at different temperatures. The trend for the minimum of *A* with increasing temperature is marked by the dashed line.

increasing temperature, trivially takes on ever more negative values, simply because ever more lattice vibrations are excited. At the same time, the molar volume of BaO expands, which we can count as a clear verification of anharmonic effects; the procedure we described as quasiharmonic (harmonically defined force constants combined with an anharmonic electronic potential) fulfills its purpose surprisingly well, and, as will be shown below, is also numerically quite reliable. Finally, we read the volume and Gibbs energy at $p = 0$ directly from the "zero pressure line", $-(\partial A/\partial V)_T = 0$. The calculation of the pressure dependence then occurs as the derivative of the state equation used in Equation (24). We would like to recapitulate the individual energy contributions once more in detail:

The total electronic energy, E_0, can be calculated routinely in the context of the so-called Born-Oppenheimer approximation[49]—that is, without any kind of atomic movement—from electronic-structure calculations of periodic solids. The

extent of the electron–electron interactions are taken into account, for example, by using density-functional theory, and, for reasons of economy, evaluated for the smallest possible unit cell, in which the convergence in reciprocal space (e.g., with the help of a set of *k*-points, as by Monkhorst and Pack[107]) is implicitly assumed. The remaining iterative energy differences are then less than 0.1 kJ mol^{-1}.

With no real additional effort, even the minor temperature dependence of the electronic excitations—so far as is absolutely necessary—can be incorporated using the approximate method by Mermin,[108] as it is already implemented in common program packages (e.g., VASP). With that step, the distribution of the electrons over the temperature-independent bands is taken into account as a function of temperature using Fermi–Dirac statistics. This correction term is negligibly small for insulators and can be omitted, but for metals it remains important. At the lowest temperatures, it leads to an extremely small heat capacity term,[35,36] that is linear with respect to temperature, which, alone among the electronic states arises in close proximity to the Fermi level. It is shown in Figure 14 for fcc-Cu.

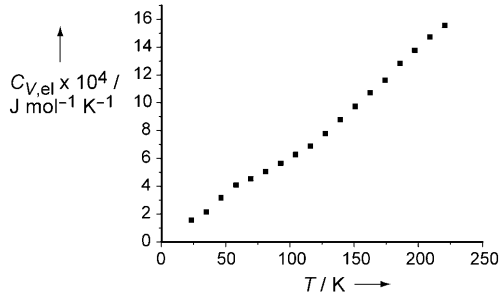

Figure 14. Density-functional-theory-calculated trend of the pure electronic aspect of the heat capacity of fcc-Cu as a function of the temperature; notice the diminutiveness and easy scattering of the five-orders-of-magnitude-smaller additional effect, which does not result from atomic vibrations.

We return to the atomic displacements: so long as we wish to treat local atomic excitations, the migration of a single atom during calculation assumes a multiple unit cell ("supercell"), and we can fully concentrate on the "path" of this migrating atom. The calculated excitation energies immediately correspond to the experimentally observed excitation energies. As soon as we consider collective excitations, however, the Hellmann–Feynman forces for all symmetry-inequivalent atomic dislocations in the supercell are necessary for the calculation of the free vibrational energy, A_{ph}. For the Direct Method, the edges of these supercells should correspond to lattice vectors of roughly equal length, and these vectors should amount to at least 8 Å.[109]

For the described (collective) approach, the following simplification is generally used: the unit cell expands only slightly with increasing temperature. Thus, an increasing temperature corresponds to a negative pressure, without taking into account the real consequences of the temperature change because, strictly speaking, all the structural degrees of freedom (lattice parameters and atomic positions) must be varied to reach the respective minima of the Gibbs energy at each temperature. Admittedly, this would result in multi-dimensional systems of equations and a hopelessly large computational effort, which, however, is usually unnecessary.

Experience shows that the vibrational energies obtained at constant volumes can simply be added to the electronic energy, from which a very good approximation for the Helmholtz energy is obtained. Often the volume-dependent trend of the vibrational energy at constant temperature is approximately linear. In these cases, the phonon calculations need not necessarily be carried out for every volume, but the already known values may be fitted by the equation $A_{ph}(V)_{T=const.} = a + bV$ from which the missing points are available. The resulting savings in computer time are quite considerable.

Figure 15 sums up, once again, the recipe for the practical implementation we have just described. The basis of all the calculations is defined fundamentally by the existing crystal

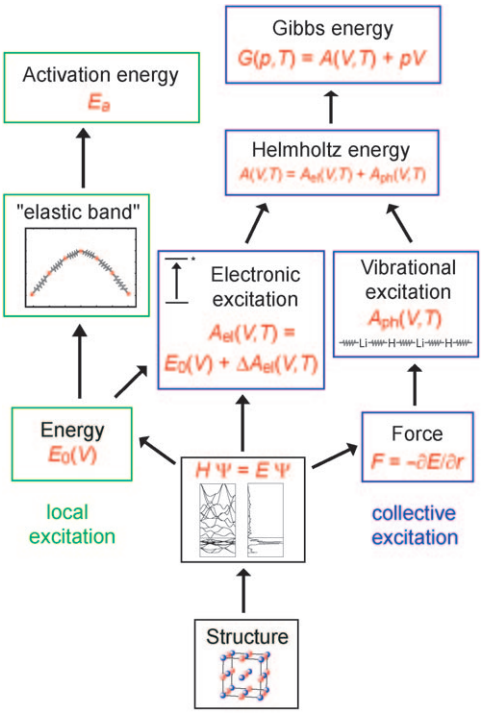

Figure 15. Flow chart of the first-principles quantum-mechanical calculation of temperature-dependent energy data from crystal structures only, with the assumption of local (left) and collective (middle and right) excitations; see also text.

structure, and all the energetic values primarily result from the solution of the (stationary) Schrödinger equation. On such an electron-theory basis, for practical reasons, it is necessary to differentiate between local (Figure 15, left) and collective (Figure 15, middle and right) atomic displacements or vibrational excitations, which, to conserve the translational symmetry, requires the use of supercells. In the local case, for example, using the NEB method is successful for the excitation energy of the migrating atom or ion whereas, in the collective case, the process starts with the forces and

moves on to the phonon energy, then to the Helmholtz energy, and finally to the Gibbs energy or free enthalpy. If G is known, then the entire thermodynamics of the system are known—the Schrödinger equation makes it possible.

5.1. Calculation of Other Thermodynamic Potentials

As previously explained, in the collective case other values besides the Gibbs energy are of great interest for the thermodynamic characterization of a system, for example the enthalpy, H, the entropy, S, and the heat capacity, C_p or C_V, yet the classical instrumentation (Legendre transformations, Maxwell relations, see Section 2.1) remains unchanged and stands ready for calculation. The entropy comes directly from the Gibbs function through the simple expression [Eq. (26)]

$$S = -\left(\frac{\partial G}{\partial T}\right)_p \tag{26}$$

and the enthalpy is accessible from the Gibbs–Helmholtz equation. The heat capacity at constant pressure, C_p, can be inferred from the calculated enthalpy or entropy, that is, accordingly [Eq. (27)].

$$C_p = \left(\frac{\partial H}{\partial T}\right)_p \text{ or } C_p = T\left(\frac{\partial S}{\partial T}\right)_p \tag{27}$$

Interestingly, C_p is related to the previously mentioned heat capacity at constant volume, C_V, by the relationship known from solid-state physics [Eq. (28)],[35,36]

$$C_p - C_V = \alpha^2 B_T V T \tag{28}$$

where α is the linear thermal expansion coefficient, B_T is the isothermal bulk or compression modulus, V is the volume, and T is the temperature. The prominent role of the Gibbs energy, exactly as is known in classical thermochemistry, makes the recourse to every conceivable thermochemical value possible. Because G is, however, accessible through recourse to the crystal structure and the solution of the Schrödinger equation, all the thermochemical questions can be addressed on a quantum-chemical basis. That this fundamental insight also, as a rule, applies numerically, we shall see below.

5.2. Data Post-Processing

The data for the thermodynamic potentials resulting from the (collective) quantum-chemical calculations must finally be fitted by functions of the type as in Equation (5) so they can be used in thermochemical databases and expert systems for thermochemical modeling. For the sake of convenience, the procedure is reverse to that of the numerical calculation of potentials; this means the first step is fitting C_p because only four parameters are necessary; the uncertainty of the fitting parameters stays as small as possible this way. Next, working with the enthalpy, H, and the entropy, S, gives successive values of the Gibbs energy, G. In these purely mathematical steps, no more physics or chemistry is involved.

5.3. Testing of an Example

In this Section we will carry out an explicit comparison with well-known, experimentally obtained thermodynamic potentials of known substances as a test for the reliability of the procedure introduced up to this point; we are first concerned with collective values only. Unless otherwise stated, the data come from the database of the Scientific Group Thermodata Europe (SGTE).[11] Among the most reliable tabulations are pure elements and binary oxides, and we limit ourselves in this case, for simplicity's sake, to the binary oxides of yttrium, barium, and copper. In Section 6, we will raise the material complexity by a large amount.

Figure 16 shows a comparison between the first-principles calculated heat capacities at constant pressure for BaO (Figure 16, top), CuO (Figure 16, middle), and Y_2O_3 (Figure 16, bottom) with data from the SGTE database. For

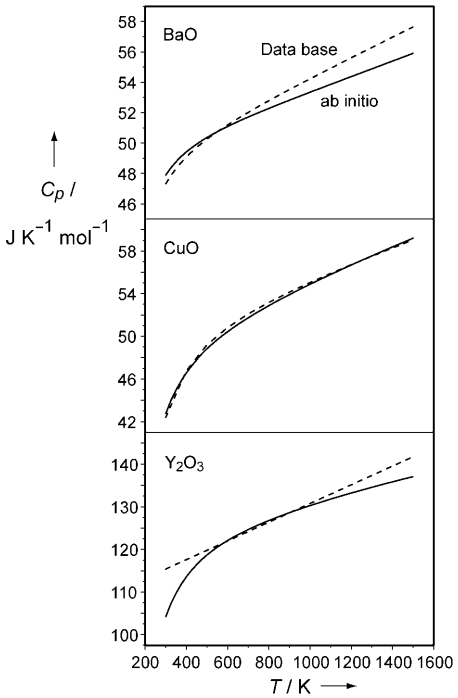

Figure 16. Density-functional-theory-calculated heat capacities of BaO (top), CuO (middle), and Y_2O_3 (bottom) as a function of the temperature at constant pressure (solid line) in comparison to the values taken from thermochemical databases (dashed).

CuO, which, for technological reasons, is the most precisely experimentally measured substance, the theoretical and experimental curves run practically congruent over the entire temperature range and thus demonstrate the high quality of the theory. The comparison for BaO is a little poorer because on the high-temperature side beyond around 600 K, theory and experiment begin to deviate from each other. It is likely that for these small differences theory must

be at fault because only a quasiharmonic model for the lattice vibrations would be taken as a basis, which must ultimately fail on approaching the melting temperature. However, even (slightly) flawed experimental values could also exist; we do not know exactly. In contrast, a very clear interpretation suggests itself for Y_2O_3 because the curve denoted "experimental" is really a completely unphysical line, and only between about 600–900 K do the theoretical and experimental curves coincide. An interpretation is clear: the tabulated heat capacity for Y_2O_3 was, by all appearances, measured once at high temperature and then extrapolated linearly to even higher and also to very low temperatures, although this ultimately leads to grossly erroneous thermochemical data for temperatures far enough removed from the temperature of measurement. This finding for Y_2O_3 is unfortunately common practice and no isolated case, and the databases even contain a few incorrect entries. On the other hand, theory offers the unique opportunity to recognize and eradicate such mistakes, and, as promised at the very beginning of this Review, to expand the measurements comprehensibly to the as yet unmeasured regions in p and T.

The comparison between the theoretical and measured entropies, S, for BaO, CuO and Y_2O_3 is somewhat better (Figure 17). For BaO (Figure 17, top), as well as for CuO (Figure 17, middle), theory and database lie very near each other; a pleasing outcome. The very incomplete experimental parameterization of Y_2O_3 is also identified by its major deviation from the theory, but it is less extreme than before.

We close this Section with a few numerical considerations. As is generally known, it is possible, at any temperature, to obtain the isothermal bulk modulus, B_T, as well as the equilibrium volume, V_T, directly from the equation of state. In addition, it may be expected that the bulk modulus decreases with increasing temperature, just because every substance softens gradually with increasing thermal energy. On the other hand, the volume at constant pressure simultaneously increases with increasing temperature, and from the gradient the expansion coefficient drawn from the volume can be easily extracted. A simple example follows:

The literature value[110] of the adiabatic bulk modulus, B_S, is about 61 ± 7 GPa for barium oxide at room temperature, and its temperature gradient $\partial B_S/\partial T$ is about -7 ± 4 MPa K^{-1}. The conversion of the isothermal bulk modulus, B_T, accessed from ab initio calculations into the adiabatic one results from the relationship of the heat capacities, C_p and C_V, according to Equation (29).

$$B_S = \frac{C_p}{C_V} B_T \tag{29}$$

The values from electron-theory calculations are about $B_S = 65.1 \pm 0.1$ GPa and $\partial B_S/\partial T = -7.9 \pm 0.6$ MPa K^{-1}, so that the deviation becomes even smaller than the simple (!) standard deviation of the experimental values. This is an extraordinarily encouraging finding, which allows us to tackle significantly more complicated applications with our theory.

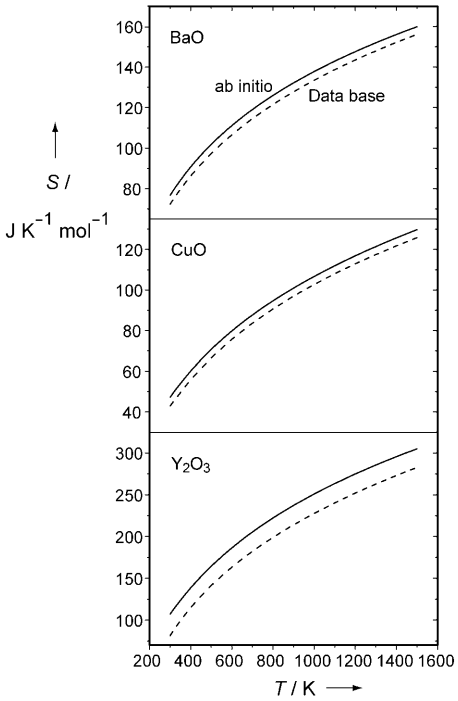

Figure 17. Density-functional-theory-calculated entropies of BaO (top), CuO (middle), and Y_2O_3 (bottom) as a function of the temperature (solid line) compared to values taken from thermochemical databases (dashed).

6. Solutions of Different Solid-State and Materials Chemistry Problems

"*Verba docent, exempla trahunt.*" ("Words instruct, illustrations lead.")

6.1. Perovskite Membranes

For the large-scale production of pure oxygen, an industrially extraordinarily important procedure, the famous Linde process is still used today. Meanwhile, however, so-called membrane processes[111] are hotly debated for the alternative operation of the power-plant process ("Oxyfuel"). To that end, people have focused on the development of new solid-state membranes, which should have a 100% selectivity to oxygen, so that the pure oxygen can be used for the complete ("pure") combustion of fossil fuels. Eventually, pure carbon dioxide is obtained as the only waste product, which in condensed form must be stored underground—and indeed until the end of time, at least that is the pious hope.

A solid-state compound with comparatively high oxygen permeability is given by the perovskite-like substance $Ba_{0.5}Sr_{0.5}Co_{0.8}Fe_{0.2}O_{3-\delta}$, which outside chemistry has the very unchemical and unaesthetic abbreviation "BSCF5582", yet we want to keep this abbreviation for the great honor of the engineers. While the common ABO_3 perovskite structure is formed of only five atoms, the composition of BSCF5582 requires the multiplication of the primitive unit cell into a supercell, and indeed in our case a doubling in all directions, accordingly; this is shown in Figure 18. With this supercell, we

have intentionally accepted a small—yet tolerable—change in the composition in the sense of a slightly different cationic sublattice (Co/Fe, see below), to save extensive computing time, which is known to scale by at least the third power of the

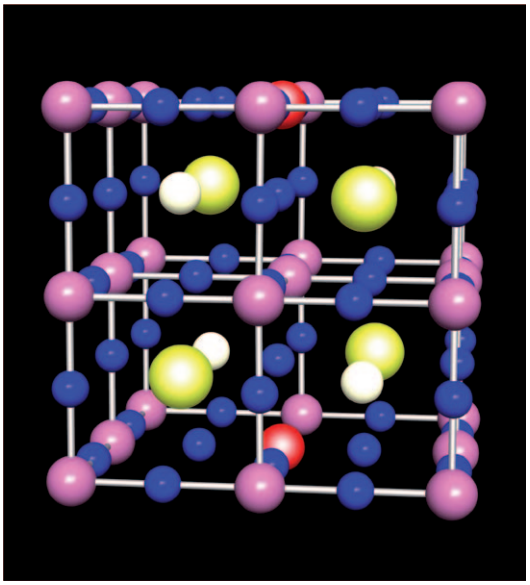

Figure 18. Perspective representation of a supercell of the approximate composition $Ba_{0.5}Sr_{0.5}Co_{0.8}Fe_{0.2}O_{3-\delta}$ ("BSCF5582"), which is created by doubling the smaller perovskite unit cell in all three directions; Fe red, Co violet, O blue, Sr white, Ba yellow.

system's size. To guarantee oxygen permeability, there must be enough oxygen vacancies in BSCF5582, and we next remove a single oxygen atom from the supercell and arrive at the composition $Ba_{0.5}Sr_{0.5}Co_{0.875}Fe_{0.125}O_{2.875}$. Now "static" density-functional theory calculations already yield that the oxygen vacancy lies preferentially near the cobalt atoms; in other words, oxygen atoms prefer to be near to iron atoms. This observation correlates with the differing oxygen affinities of the two elements iron and cobalt, since the free formation enthalpy of the oxide MO at 1600 °C is significantly larger for iron ($\Delta G_f = -147\ kJ\,mol^{-1}$) than for cobalt ($-101\ kJ\,mol^{-1}$).[112]

To make a quantum-mechanical conclusion about the flow of oxygen through a membrane of BSCF5582, we calculate the activation energy for the migration of a single oxygen atom through the crystal, in our case with the help of the NEB method. The migrating oxygen atom experiences a quasi-octahedral (4+2) coordination by the cations in the beginning and ending steps as a result of the perovskite motif. In the course of the hopping movement, the oxygen atom must fit through a triangular face which is spanned by two neighboring octahedra. The beginning and ending positions of the oxygen atom are shown in Figure 19. To save significantly on computation time, only the position of the migrating oxygen atom and the first-nearest neighbors of the triangular face are allowed to relax during the NEB optimization of the jump path. The energy profile for two given NEB calculations, which differ in the composition of the triangular face, are

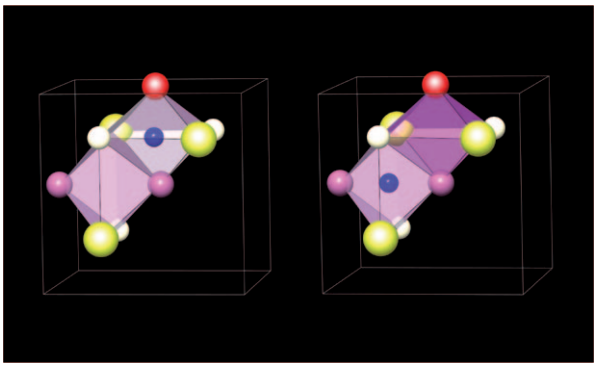

Figure 19. Oxygen hopping from an O-containing octahedron (left) into a free neighboring vacancy (right) of "BSCF5582"; Fe red, Co violet, O blue, Sr white, Ba yellow. The O atom is first coordinated by one Fe and one Co atom (Fe-O-Co), after hopping it is coordinated by two Co atoms (Co-O-Co).

presented in Figure 20. A saddle-point configuration is formed from a strontium, a barium, and a cobalt atom, hence called Δ_{SrBaCo}; in the other, the Co atom is exchanged by one Fe atom (Δ_{SrBaFe}). The course of the curves can be understood on the basis of effective coordination numbers

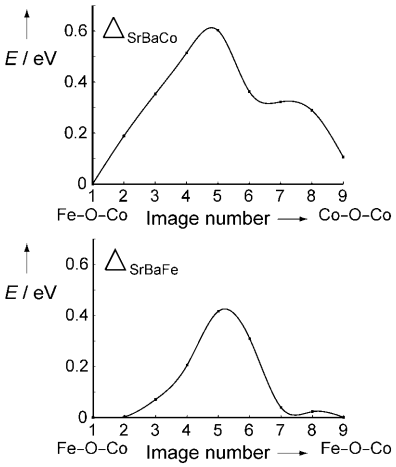

Figure 20. Activation energies of the oxygen-hopping process for two different saddle-point configurations, Δ_{SrBaCo} and Δ_{SrBaFe}, calculated on the basis of the NEB method; see the text for further details.

(CN_{eff}) according to Brunner and Schwarzenbach,[113] this is because in Figure 20 the intermediate step with the smallest CN_{eff} also exhibits the highest energy. The comparison of both energy barriers similarly shows that the barrier in the presence of Co is a little larger (about 0.6 eV) than for Fe (about 0.4 eV). The higher affinity of O for Fe that we know from the macroscopic free MO formation enthalpy can be detected in this case inasmuch as the configuration Fe-O-Co (Figure 20, image number 1) is energetically about 0.1 eV lower than the configuration Co-O-Co (Figure 20, image number 9).

In connection with Figure 20, we have applied an additional computational maneuver, without which the two curves

would show a massive (and completely non-physical) maximum at image number 8; it is at least tentatively recognizable in both curves. Upon dislocating a single atom, all other lattice parameters, as well as the volume of the unit cell, must of course be reconverged by electronic-structure theory, otherwise a non-physical internal structural pressure or strain arises, which shows up seriously in the size of the energy barriers. Without a manual readjustment of the metric of the unit cell, these drop out significantly higher (at least 1.3 eV) and then deviate strongly from experiment. From permeability measurements, however, activation energies of about 0.5 eV have been derived,[114] in very good agreement with our values. The slight deviation (ca. 0.1 eV) between ab initio calculations and experimental measurements is therefore quite striking because it cannot be assumed throughout that similar oxygen vacancy concentrations exist in theory and experiment. These concentrations are known exactly in theory from the principle knowledge of the simulation cell, but in experiment they are frequently approximate. It is notoriously nontrivial to ascertain the exact oxygen composition of the real material, and many transport measurements are carried out under the assumption that the primarily desired composition was achieved upon synthesis. Apparently, the size of the activation energy of BSCF5582 is a "good-natured" property.

6.2. Silver Bis(propinyl)argentate(I)

From the exploratory solid-state chemistry, it is long known that compounds of transition metals containing alkyne groups are recognized or even notorious for their thermal instability; some of these substances can abruptly disintegrate and explode. In this Section we will concentrate on the comparatively harmless silver bis(propinyl)argentate(I), which consists of univalent silver cations and complex anions of the composition $[Ag(C_3H_3)_2]^-$. Already nearly 50 years ago, Nast and co-workers were the first to produce such complex anions in pure form.[115,116] The characterization of the material succeeded, in the absence of available single crystals, on the basis of elemental analyses and the characteristic chemical behavior. Even today, no practicable way is known to attain single crystals, so the structure solution must be based on powder data and subsequent Rietveld refinements. Owing to the very large differences in the scattering power of the atoms, however, the principle limits of the procedure are approached, even using intense synchrotron radiation and high-resolution diffraction patterns because very different structure models—with respect to the local Ag coordination of the central structural unit $[Ag(C_3H_3)_2]^-$—do not differentiate themselves significantly enough with respect to the figure of merit[117] needed to guarantee a reliable structural elucidation.

For the clarification of the structural motif, we show a section from the crystal structure finally realized to be correct in Figure 21, which was achieved using high-resolution X-ray diffraction, infrared spectroscopy, and ab initio calculated vibrational spectra (our contribution). Precisely for these kinds of substances can IR spectroscopy supply important

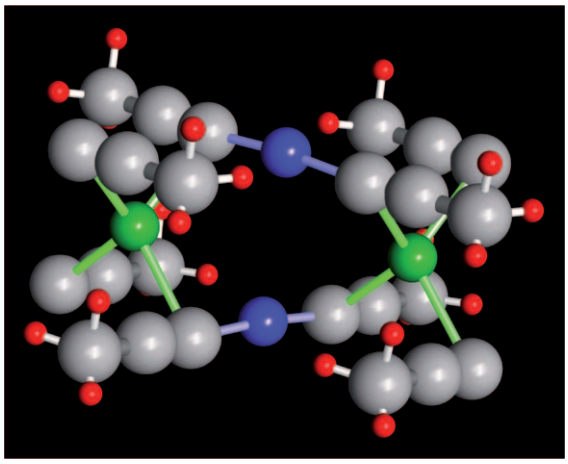

Figure 21. Perspective representation of a section of the structure of silver bis(propinyl)argentate(I) with the linear coordination ($d = 2.0$ Å) of silver (blue) by carbon (gray) in the complex anion $[Ag(C_3H_3)_2]^-$. Another silver atom (green) with a tetrahedral coordination environment bonds ($d = 2.5$ Å) "side-on" to the propinyl unit.

conclusions about the arrangement of the organic groups in the crystal. This is because the existence of single, double, or triple bonds as well as, especially important, the bonding of the propinyl group to the silver atom can be clarified by the assignment or characteristic shift of the bands in the IR spectrum. IR spectroscopy actually offers X-ray diffraction a helping hand, an unusual insight for the solid-state chemist.

Nonetheless, the assignment of the vibrational modes in extended solids is not always unambiguously simple because—in contrast to organic molecular chemistry—the necessary reference substances are simply lacking. On the basis of quantum-chemical calculations of a solid, however, the IR spectrum of the compound can be simulated freely. It is necessary, in turn, to rely on the calculation of the collective lattice vibrations, which are accessible with the help of plane waves, PAW pseudopotentials, and the GGA. It can be shown that the phonon density of states (pDOS) is directly coupled with the experimental vibrational spectrum; as previously explained, the pDOS reflects the number of vibrational states as a function of the energy or frequency, in analogy to the electronic density of states. Likewise, the number of vibrational states may be plotted as a function of the wavenumber to make the direct comparison with experimental vibrational spectra possible, and this is shown for the example of silver bis(propinyl)argentate(I)[118] in Figure 22. Exactly as in the experimental spectrum, the individual vibrational modes can be assigned precisely from the pDOS, and this either through looking at the vibrating atoms on the computer monitor or through considering the output of the atom-projected pDOS. In this way the IR signal at a wavenumber of about 2100 cm^{-1} is well-characterized as a typical valence vibration of a C≡C triple bond with slightly lowered electron density, as a result of the "side-on" coordination of Ag to the π-system. On the other hand, for example, the bands for C–H deformation vibrations are typically found at a wavenumber of about 1400 cm^{-1},[119] as in our case. When not only the internal quality criteria of the X-ray crystallographic structural

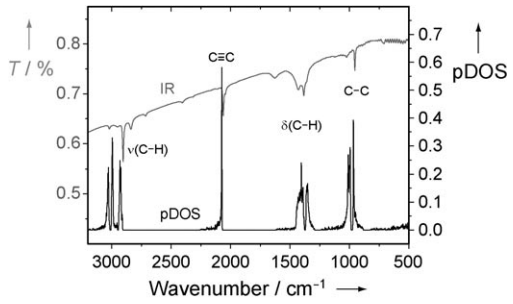

Figure 22. Ab initio calculated phonon density of states (pDOS; bottom) of solid silver bis(propinyl)argentate(I) and an experimental IR spectrum (top) of the substance.

determination turn out to be reasonable but also the theoretically predicted vibrational properties of the compound, on the basis of this same crystal structure, completely agree with the experiment, the crystal structure is finally verified.[117]

6.3. Tin Pest

Hardly any other temperature polymorphism of solids has been treated more often in textbooks of structural chemistry[120,121] than the transition from white to gray tin. Even in introductory courses one learns that the main-group metal tin experiences a transformation when it falls below a temperature of 13.2 °C, from the very dense β polymorph ($\rho = 7.29\ g\,cm^{-3}$) into the diamond-like, half-metallic and significantly looser α polymorph ($\rho = 5.77\ g\,cm^{-3}$). The coordination number also reduces from 4 + 2 ($d = 3.02$ and 3.18 Å) to 4 ($d = 2.81$ Å). Owing to the enormous density difference, this usually results in catastrophic material failure; the term "tin pest" speaks for itself.

In Figure 23 we introduce the results of conventional electronic-structure theory but still without involving finite temperatures. The plot of the relative enthalpy at absolute zero versus the pressure immediately reflects the stability of the less dense α phase, and indeed by about 3.7 kJ mol^{-1}. Not until a theoretically predicted transformation pressure of about 0.7 GPa would α-Sn transform into the metastable but denser β polymorph, because beyond this pressure it has the lower enthalpy (Figure 23, dashed). This value fits very well with the experimental transformation pressure of about 1 GPa[122] and also to earlier, independent calculations, which predicted 0.9 GPa.[123]

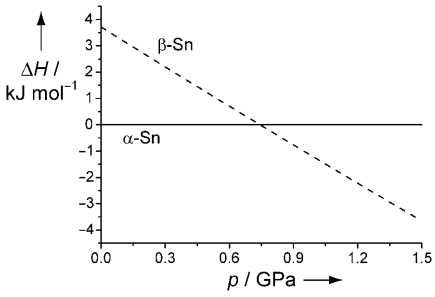

Figure 23. Density-functional-theory-calculated relative enthalpies of α-Sn (solid line) and β-Sn (dashed) as a function of pressure without inclusion of the temperature.

The calculation of the relative Gibbs energies at finite temperatures is today, a few years later, relatively easy to carry out, namely on the basis of supercells for the phonon spectra of both polymorphs if only plane waves, pseudopotentials, and the generalized-gradient approximation are used. For α-Sn a 4 × 4 × 4-fold supercell was used, for β-Sn a 4 × 5 × 4-fold supercell, so that this first step significantly slows the calculation (see Section 4.1).[124] If the absolute Gibbs energy of the diamond-like tin is then set to zero as a reference value (baseline), this results in the diagram of relative G functions as shown in Figure 24, which actually

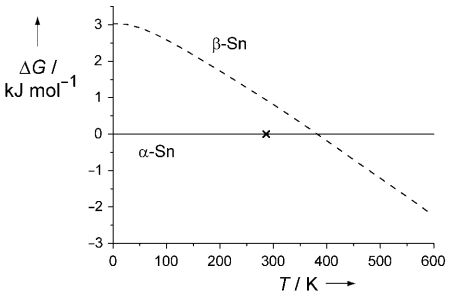

Figure 24. Density-functional-theory-calculated relative Gibbs energies of α-Sn (solid line) and β-Sn (dashed) as a function of the temperature; the experimentally known transition temperature (cross) is marked for comparison.

indicates the α polymorph as the more stable phase at low temperatures, once again. The first-principles calculated transition temperature lies only about 90 K higher than the experimental value (Figure 24, cross), which corresponds to an energetic error of less than 8 meV or 0.8 kJ mol^{-1}; such precision for solid-state calculations would have been downright unthinkable until recently, and eventually it could still improve a little through the addition of anharmonic effects.

On the other hand, we may directly compare the heat tone (that is, the experimental enthalpy of transformation) at the experimental transformation temperature. The experimental value lies around 2 kJ mol^{-1},[125] whereas the theoretical value for ΔH_{300K} amounts to about 3.6 kJ mol^{-1}, which again gives an impressive mutual verification of experiment and theory. Clearly the first-principles quantum-mechanical calculation can almost compete with experiment, although the computational demand of the thermochemical calculation for the structurally relatively simple α-Sn, compared with a single band-structure calculation, takes two to three orders of magnitude more time, depending on system and problem. In practice this situation means that today the calculation of the enthalpy–pressure curve presents practically no problem any more, and the significantly more laborious G-temperature curve is best carried out on a computer cluster, so that, in the case of tin, it is finished within a week, on a supercomputer even within just one day. Larger and more complicated systems require a corresponding time. This calculation is

presumably faster than the measurement, which calls for the clean preparation of the experimental object, the calibration of the measuring device, and a lot more.

6.4. Oxynitrides

The majority of all binary solid-state compounds are oxides; next to them, is an at least two orders of magnitude smaller number of nitrides. Only within the last two decades, however, interest has turned to the so-called oxynitrides[126,127] because their properties can be so superbly controlled through the O:N ratio. For this reason, these phases lend themselves to custom-made pigments,[128] dielectrics,[129] and also for catalysts.[130,131]

The archetype of all oxynitrides is given, without any doubt, by TaON, whose thermodynamically stable β polymorph[132,133] is distinguished by a sevenfold Ta coordination with a perfectly ordered O/N sublattice[134] and which was shown in quantum-chemical calculations to have a perfectly balanced bonding situation,[135] in contrast to a non-existent α polymorph and a similarly conceivable high-pressure phase.[136] In addition, since very recently there is an exciting new metastable polymorph (γ-TaON), in which the Ta atom is surrounded by O and N atoms in the motif of a distorted octahedron.[137] Figure 25 displays both polymorphs, whereby the noticeably more open character of the γ-TaON clearly comes to light.

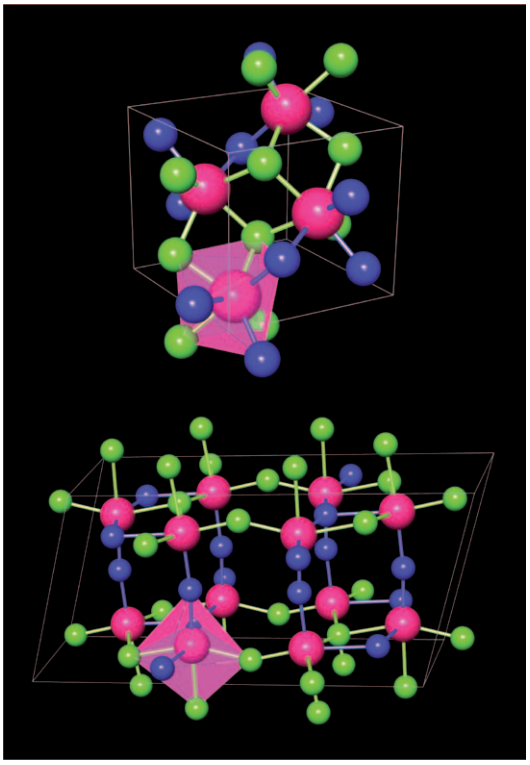

Figure 25. Perspective representation of the crystal structure of β-TaON (top) and of γ-TaON (bottom) with Ta red, O blue, and N green. Although the Ta atom is seven-coordinate in the β polymorph, the less-dense γ polymorph has a distorted octahedral Ta coordination.

Shortly after the discovery of γ-TaON, electronic-structure calculations on the basis of complimentary approaches (Hartree–Fock as well as DFT; local orbitals as well as plane waves) suggested the metastable character of this phase, in accordance with experiment.[137] Systematic theoretical investigations finally showed[138] that γ-TaON is positioned energetically around 20 kJ mol^{-1} above the stable polymorph and therefore must spontaneously transform into it. The same conclusion is provided by the ab initio calculated phonon spectra of both phases of TaON, which are given in Figure 26.

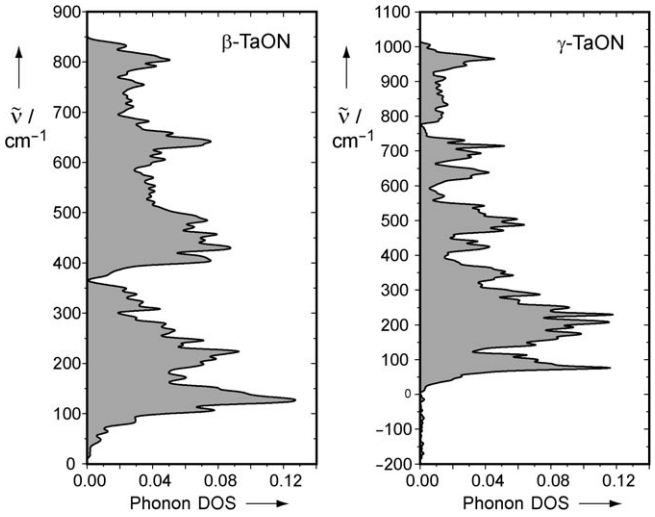

Figure 26. Density-functional-theory-calculated phonon density of states of two polymorphs of tantalum oxynitride; β-TaON (left), γ-TaON (right). The imaginary modes for γ-TaON are shown as negatives.

These indicate imaginary wavenumbers only for the γ polymorph, which for obvious reasons usually, and also herein, are represented as negative values. The term "soft modes" is known from physics, when frequencies fall to zero upon getting extremely close to a phase transformation.[139] In this particular case, however, the frequencies are actually imaginary, a clear indication of spontaneous (although in reality unnoticeably slow) decomposition. The compound is inherently unstable, and the solid-state calculation demonstrates it directly in consideration of the collective vibrational states.

Since γ-TaON unfortunately cannot be synthesized phase-pure yet, the desired temperature–pressure phase diagram is preferably calculated by ab initio methods than measured experimentally. It is shown in Figure 27 and presents the new phase relative to the normal phase. At a given temperature, increasing the pressure on γ-TaON must always lead to the denser β-TaON phase, analogously to the case of tin. In good agreement with the pressure–coordination-number rule, the coordination number for Ta increases from six in γ-TaON to seven in β-TaON. Finally, the bulk modulus for γ-TaON also comes out about 35% smaller, simply because the structure contains so many "holes".

The explicit temperature dependence of the calculations, however, additionally shows that a temperature of about 570 K must lead to a distinct destabilization of β-TaON which

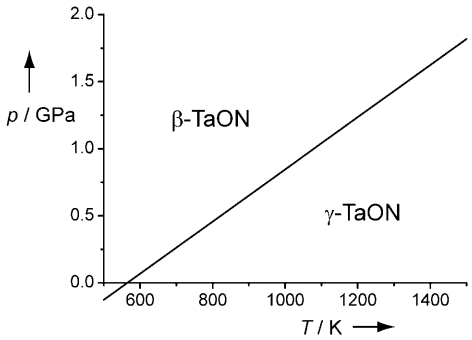

Figure 27. Density-functional-theory-calculated pressure–temperature phase diagram for β-TaON (ground state) and the metastable phase γ-TaON.

then makes it energetically equal to γ-TaON. The equilibrium phase line between both polymorphs runs practically linearly and thereby separates the stable high-pressure phase (Figure 27, top left) from the metastable open phase (Figure 27, bottom right). Only the first-principles calculation allows the creation of such an equilibrium diagram, and indeed without any thermochemical measurement. These measurements would be quite feasible for β-TaON, but γ-TaON, which can be made only in low yields, is chronically contaminated with other phases, and to this day cannot be prepared cleanly—and therefore also cannot be measured reliably.

6.5. Superconducting Cuprates

About twenty years ago, one of the most fascinating areas of solid-state chemistry, as well as physics and materials science, was opened with the discovery of high-temperature superconductivity in oxocuprates.[140] Probably the best-known compound of this family of materials is the so-called yttrium–barium–cuprate $YBa_2Cu_3O_{7-x}$ or "Y123" for short,[141] simply because this phase, with its critical temperature of about 93 K (for $x = 0$), allowed superconductivity with liquid-nitrogen cooling (boiling point: 77 K) for the first time. At the present time, there is still no apparent theoretically conclusive, let alone fully accepted, description of this special form of superconductivity,[142] presumably because the high chemical complexity of the compounds[143] plainly overcomes our understanding, so that the prediction of the compositions of new superconductors appears to be absolutely impossible right now.

Figure 28 shows a view of the crystal structure of the orthorhombic phase of $YBa_2Cu_3O_{6.5}$ with $T_C \approx 60$ K, which has two-dimensional CuO_2 layers parallel to the *ab* plane with divalent Cu and one-dimensional alternating CuO_3 and CuO_2 chains along the *b* axis with tri- and monovalent Cu;[144] precisely these chains serve as charge reservoirs for the superconducting layers.[145] Unfortunately, there is also a tetragonal polymorph of this composition, in which the ordering of the chains along *b* is lost, and this phase, which is to be avoided experimentally, shows no superconducting properties whatsoever. For this reason, thermodynamic considerations for large-scale production of superconductors using wet chemical precipitation on textured metal bands play an extremely important role.[146] Admittedly, the thermochemical databases prove to be fragmentary once again.

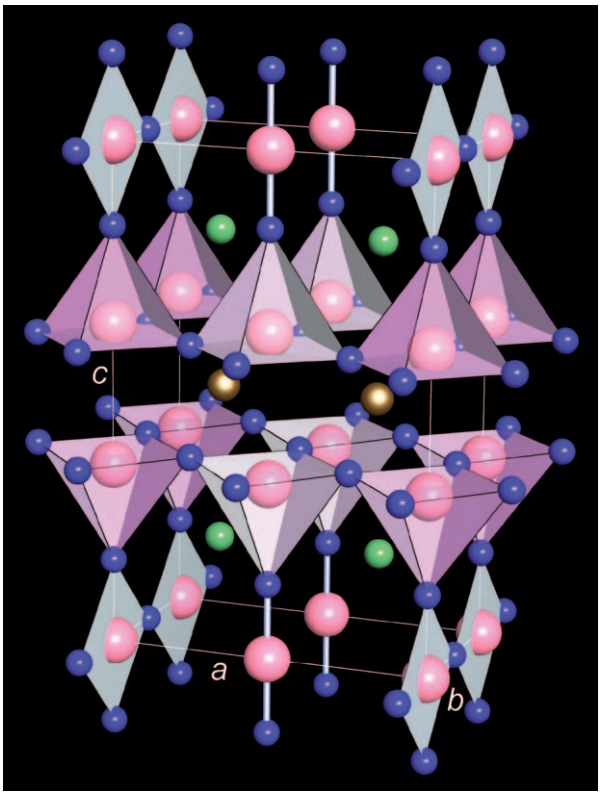

Figure 28. Perspective representation of the crystal structure of orthorhombic $YBa_2Cu_3O_{6.5}$ with Y gold, Ba green, Cu red, and O blue; the superconductivity occurs in the two-dimensional CuO_2 layers in the *ab* plane, whereas the one-dimensional CuO_3 and CuO_2 chains serve as an electronic reservoir for the layers; see text for further details.

Through first-principles calculations above the critical temperature, we are now in a position to illuminate the phenomena from a fresh perspective, admittedly by accepting certain theoretical approximations, but under strict exclusion of any experimental errors or intricate kinetic problems for such complicated systems. Figure 29 shows a calculated Gibbs energy–temperature diagram for the aforementioned phase transition between orthorhombic and tetragonal $YBa_2Cu_3O_{6.5}$, and it is based solely on quantum-chemical principles. Additionally, the influence of the configurational entropy, which concerns the distribution of the O atoms in the one-dimensional chains, is included. Of course, intuitively a higher stability is expected at higher temperature for the tetragonal phase because the ordering of the O atoms in the chains can no longer be sustained, and this expectation is fulfilled. The calculated transition between both phases is about 775 K and can be compared with the experimentally described one (about 800 K); the latter appears to be rather imprecise, particularly since experimental difficulties (kinetics!) complicate the determination. Additionally, the theoretical knowledge of the *G* differences over the full temperature range allows the equilibrium distribution between

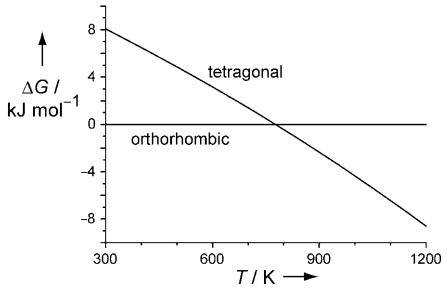

Figure 29. Density-functional-theory-calculated relative Gibbs energies for the tetragonal and orthorhombic polymorphs of $YBa_2Cu_3O_{6.5}$; the phase transition is predicted at a temperature of approximately 775 K.

orthorhombic and tetragonal phases to be stated quantitatively for a chosen temperature.

Yet even when we focus on fundamental thermochemical information, such as the Gibbs energy for the formation of orthorhombic $YBa_2Cu_3O_{6.5}$, the strengths of the theory are already impressively demonstrated. For example, the free reaction enthalpy of this and similar phases have been measured most carefully, and the recent IUPAC report[147] contains an empirical Gibbs function for this compound with a total of 16 (!) parameters, in which a total of 3300 (!) data points from 240 (!) different, skillfully conducted experiments were fitted, naturally after a previous (subjective?) estimation of the goodness of all of these data points and measurements. The result is depicted in Figure 30, namely the above-mentioned free enthalpy of formation of orthorhombic $YBa_2Cu_3O_{6.5}$ (Figure 30, solid curve). At the same time, the upper and lower accuracy limits (Figure 30, dotted) are

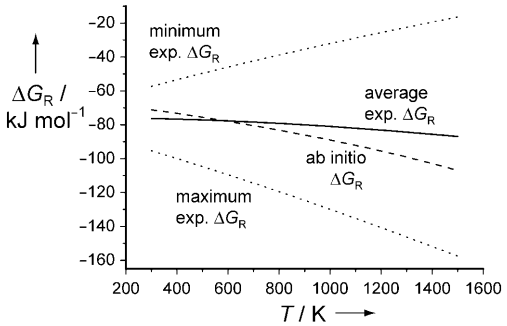

Figure 30. Density-functional-theory-calculated (dashed) free formation enthalpy, ΔG_R, of the orthorhombic polymorph of $YBa_2Cu_3O_{6.5}$ and experimental literature values (solid); the upper and lower limits of accuracy of the experimental values are also marked (dotted).

indicated for a certainty of 99%, and these tend to be surprisingly broad, possibly because of experimental difficulties or conflicting data. How accurate is the experimentally determined value of ΔG_R really?

Instead of preparing new samples and collecting additional experimental data, we can calculate the free enthalpy of reaction by ab initio methods. It requires the electronic-structure theory of all the phases that are present in the following equilibrium; in this case there are just the binary oxides Y_2O_3, BaO, and CuO in their stable polymorphs. The reaction to be calculated is

$$^1/_2\,Y_2O_{3(s)} + 2\,BaO_{(s)} + 3\,CuO_{(s)} \rightleftharpoons YBa_2Cu_3O_{6.5(s)}.$$

The theoretical effort is enormous, but it must be executed in full only once. In our computational practice (that is, with a combination of a computer cluster and a supercomputer) it was equivalent to computing resources of one week per reactant and one month for the $YBa_2Cu_3O_{6.5}$ phase itself. The ultimately resulting theoretical Gibbs function (free reaction energy or free energy of formation) is also displayed in Figure 30, dashed line, and it runs relatively close to the experimental mean. The tendency of experiment and theory is fairly similar, but which of the two provides higher reliability has yet to be seen. We trust our G function to be, in the worst case, more accurate than $\pm 10\ kJ\,mol^{-1}$, and that over the entire illustrated temperature range.

7. Outlook

The previous demonstrations show quite strikingly that, at least in our opinion, a first-principles, and generally numerically reliable, calculation of thermochemical material properties is achievable now, insofar as it is based on fundamental electronic-structure theory and incorporates lattice-dynamics interactions. We stand by the fact that for a structurally well-characterized material the theory proves itself to be a most serious competitor to the experiment, and we also predict that this welcome development will raise the significance of thermochemical approaches in daily research. Of course, it is much easier to prepare, for the second time, a clean sample of a recently unknown but now crystallographically characterized phase once its thermochemical properties can be calculated—solely based on the electronic structure—from the crystal structure alone. The synthetic chemists will soon profit greatly from the theory.

On the other hand, the existing and future problems to solve are very clear. The theoretical pitfalls may lie in the ab initio theory of the electronic states themselves and in the theoretical treatment of the atomic displacements, whether local or collective (phonons). As far as the collective excitations are concerned, the real, existing interatomic potential is known to be always anharmonic, and the usually well-behaved quasiharmonic approximation finally collapses at temperatures near the melting point. Obviously, the anharmonicity of the lattice vibrations using ab initio molecular-dynamics methods[148] can be included almost exactly, though the computing time required for the desired accuracy would be gigantic. The alternative, and recently published first attempt for aluminum, is to calculate thermodynamic potentials including the anharmonicitiy and also the defect formation (!) based solely on density-functional theory;[149] it does look successful but requires the introduction of a Langevin dynamics for reducing the computing time. Nonetheless, the thermodynamic corrections beyond the quasiharmonic approximation turn out to be tiny, as might be expected; whether the huge expense is worthwhile, remains to be seen from case to case. For itinerant-magnetic solids such as the numerous Heusler alloys,[150] it has recently been shown how collective magnetic excitations—density-func-

tional theory is, unfortunately, not accurate enough for the ab initio prediction of the Curie temperatures[151]—can be included in the free energy if empirical information is added;[152] again we are concerned with extremely small correction contributions. The challenges are great, however, we consider that they are not critical owing to the (very) small errors.

Unfortunately, the nearly omnipresent density-functional theory itself shows, for some solids, ugly weaknesses which manifest themselves, for example, in the energetically false estimate of multiple bonds,[153] the notorious unreliability for weak interactions (e.g., van der Waals forces)[154] and, quite generally, in the numerous problems of so-called "correlated" electronic states,[155] as is particularly frequently found for d- and f-metals. Although for these metals, semi-empirically looking corrective methods (with an effective Hubbard parameter, for example GGA + U) are common practice,[156,157] yet there are also systems for which no ad hoc method for simple DFT correction is available.[158] At this point, in fact, a broad field opens for the wave-function-based quantum chemistry of solid matter to describe the thermochemistry even of crystals composed of molecules in a quantitatively correct manner. This should be considered especially whenever the periodic wave function may be composed of strictly localized group functions, which serve as a quantum-chemical mirror image of the chemical structure.[159,160]

Even if no revolutionary improvement of electronic-structure theory can be expected, we predict—owing to the continuously growing computing power and the already achievable accuracy—the following developments: Within the next few years, it will become routine to calculate G functions and also pressure–temperature diagrams with good accuracy, simply because it vastly increases our knowledge of novel compounds and materials, and the calculation can already be faster than the measurement; with the knowledge of G, synthetic attempts will always be more rational. If classical thermochemical approaches (e.g., sublattice models[11] and similar tactics) can be linked even more strongly with the ab initio theory, then there is nothing against the creation of multidimensional G functions, which directly depend not only on temperature, but also on the chemical composition and other parameters. We are convinced that in roughly one decade we may rationally perambulate the multidimensional G space using some help from computers in the search for new materials. Finally, the procedures will become so powerful that eventually even highly complex, industrially relevant questions (e.g., slags and other weird mixtures) can be addressed, yet there remains much to do even for the fundamentals. We know that some geoscientific questions (such as, for example, processes in the earth's crust or mantle) can be solved only with the help of theory,[161] in particular using a concerted effort between thermochemistry, quantum chemistry, solid-state physics, and solid-state chemistry.

Appendix A: Computational Methods

The quantum-chemical calculations were carried out predominantly with the VASP package[82] based on plane waves. Exchange and correlation were, as a rule, taken into account by the GGA functional by Perdew, Burke, and Ernzerhof (PBE),[96] and in individual cases with the LDA functional by Ceperly and Alder.[162] The separation of core and valence electrons was performed with the help of the projector-augmented wave method (PAW).[80] The control of all electron-theoretical procedures was carried out with a multipurpose tool,[163] the calculations of the phonons, in contrast, with the help of the FROPHO program,[164,165] while the forces required for the calculation of the force constants were likewise obtained from VASP. The subsequent conversion of the energy data obtained from electronic-structure theory into thermochemical potentials and their incorporation or adjustment into the thermochemical databases besides their numerical and graphical processing was done with a set of customized scripts.[166] The perspective structure diagrams were created with the program Balls & Sticks.[167]

Appendix B: Mathematical Supplement

Dynamical Matrix

The so-called dynamical matrix, D, tabulates all forces occurring in the system in a compact form, and it is calculated by the Fourier transformation of the force-constant matrix according to the Equation (30)

$$D_{\alpha\beta}(\mathbf{k}) = \frac{1}{\sqrt{mm'}} \sum \Phi_{\alpha\beta} e^{i\mathbf{k}[\mathbf{r}'-\mathbf{r}]} \tag{30}$$

Subsequently, the secular determinant is set equal to zero [Eq. (31)]

$$\left| D_{\alpha\beta}(\mathbf{k}) - \delta_{\alpha\beta}\delta_{kk'}\omega^2(\mathbf{k}) \right| = 0 \tag{31}$$

and all of the sought-after phonon frequencies, ω, can be obtained as solutions in one step.

Partition Function and Phonon Energy

The free phonon energy, A_{ph}, runs proportional to the absolute temperature and to the natural logarithm of the partition function, that is, according to Equation (32).

$$A_{\mathrm{ph}} = -k_{\mathrm{B}}\, T \ln Z \tag{32}$$

For the calculation of the partition function it is necessary to sum over all temperature-dependent harmonic phonon energies [Eq. (33)].

$$Z = \sum_j e^{-E_{\mathrm{ph},j}/k_\mathrm{B}T} \tag{33}$$

Simplified Equation of State

The equation of state derived from Hooke's law by Murnaghan describes the energy–volume function of a solid in a simplified form according to Equation (34),

$$E(V) = E(V_0) + \frac{B_0 V}{B_0'}\left[\frac{(V_0/V)^{B_0'}}{B_0' - 1} + 1\right] - \frac{B_0 V_0}{B_0' - 1} \tag{34}$$

where V_0 is the volume at E_0, and B_0 is the bulk modulus in the ground state; B_0' is the dimensionless derivative of $B(V)$ at V_0.

Note Added in Proof

While the proofs for this Review were being prepared, our attention was drawn to a publication by De Souza and Martin[168] who performed, for the related perovskite-like compound $LaGaO_3$, force-field calculations targeted at the activation energy of the oxygen mobility. The independent findings concerning the chemical composition of the triangular configuration upon oxygen jump are in good agreement with our results (section 6.1) and they also emphasize the percolative character of the long-range oxygen transport. Because of this character, the activation energy does not depend too much on the actual number of oxygen vacancies.

We would like to thank the German Research Foundation (DFG), the Federal Ministry for Research and Technology (BMBF), the Helmholtz Alliance "MEM-BRAIN", as well as the Federal Ministry for Economy (BMWi) for the financial sponsorship of our work, Professor Klaus Hack (Gesellschaft für Technische Thermochemie und -physik, Herzogenrath; GTT) and Professor Andrei Tchougréeff (Lomonosow University, Moscow) for helpful comments as well as the computer centers of RWTH Aachen University, the research center at Jülich and the Technical University of Stuttgart for the generously provided computing time.

Received: December 1, 2009
Published online: June 22, 2010
Translated by: Beth Leverett Haas, Ann Arbor

[1] A. R. West, *Solid State Chemistry and its Applications*, Wiley, New York, **1984**.
[2] A. R. West, *Basic Solid State Chemistry*, Wiley, New York **1997**.
[3] L. Smart, E. Moore, *Solid State Chemistry: An Introduction*, 2nd ed., Chapman & Hall, London **1995**.
[4] A. K. Cheetham, P. Day, *Solid State Chemistry: Techniques*, Clarendon, Oxford **1987**; *Solid State Chemistry: Compounds*, Clarendon, Oxford, **1992**.
[5] R. J. D. Tilley, *Understanding Solids: The Science of Materials*, Wiley, New York, **2004**.
[6] G. Tammann, *Z. Angew. Chem.* **1926**, *39*, 869.
[7] J. A. Hedvall, *Reaktionsfähigkeit fester Stoffe*, Johann Ambrosius Barth, Leipzig, **1938**.
[8] K. Hauffe, *Reaktionen in und an festen Stoffen*, 2nd ed., Springer, Berlin, **1966**.
[9] H. Schmalzried, *Solid State Reactions*, 2nd ed., Verlag Chemie, Weinheim, **1981**.
[10] O. Kubaschewski, C. B. Alcock, *Metallurgical Thermochemistry*, 5th ed., Pergamon, Oxford, **1979**.
[11] K. Hack, *The SGTE Casebook*, 2nd ed., Woodhead, Cambridge, **2008**.
[12] J. W. Gibbs, *Trans. Conn. Acad. Arts Sci.* **1876**, *3*, 108.
[13] E. A. Guggenheim, *Proc. R. Soc. London Ser. A* **1935**, *148*, 304.
[14] K. K. Kelley, *Bull. U. S. Bur. Mines* **1949**, *476*.
[15] A.-T. Petit, P.-L. Dulong, *Ann. Chim. Phys.* **1819**, *10*, 395.
[16] A. Einstein, *Ann. Phys.* **1907**, *22*, 180.
[17] G. Ahlers, *Rev. Sci. Instrum.* **1966**, *37*, 477.
[18] G. K. White, S. J. Collocott, *J. Phys. Chem. Ref. Data* **1984**, *13*, 1251.
[19] The truly present T^3 law of the heat capacity of real substances at low temperatures can be demonstrated nicely in atomic crystals (for example, crystalline argon).
[20] P. Debye, *Ann. Phys.* **1912**, *344*, 789.
[21] P. W. Atkins, J. de Paula, *Atkins' Physical Chemistry*, 7th ed., Oxford University Press, **2001**.
[22] G. Wedler, *Lehrbuch der Physikalischen Chemie*, 4th ed., Wiley-VCH, Weinheim, **1997**.
[23] Because the nature of the chemical bond determines the interatomic force constants, the chemical bond, naturally, is reflected in the heat capacities, and indeed as the departure from the rule by Neumann and Kopp.[21,22]
[24] G. A. Landrum, R. Dronskowski, *Angew. Chem.* **2000**, *112*, 1598; *Angew. Chem. Int. Ed.* **2000**, *39*, 1560.
[25] M. Bredol, U. Kynast, C. Ronda, *Chem. Unserer Zeit* **1994**, *28*, 36.
[26] W. J. Moore, *Seven Solid States*, Benjamin, New York, **1967**.
[27] R. Imbihl, A. Scheibe, Y. F. Zeng, S. Günther, R. Kraehnert, V. A. Kondratenko, M. Baerns, W. K. Offermans, A. P. J. Jansen, R. A. van Santen, *Phys. Chem. Chem. Phys.* **2007**, *9*, 3522.
[28] A. Tunde Raji, S. Scandolo, R. Mazzarello, S. Nsengiyumva, M. Härting, D. T. Britton, *Philos. Mag.* **2009**, *89*, 1629.
[29] "Methods for Finding Saddle Points and Minimum Energy Paths": G. Henkelman, G. Jóhannesson, H. Jónsson in *Progress in Theoretical Chemistry and Physics* (Ed.: S. D. Schwartz), Kluwer, Dordrecht, **2000**, pp. 269–300.
[30] "Nudged Elastic Band Method for Finding Minimum Energy Paths of Transitions": H. Jónsson, G. Mills, K. W. Jacobsen in *Classical and Quantum Dynamics in Condensed Phase Simulations* (Eds.: B. J. Berne, G. Ciccotti, D. F. Coker), World Scientific, Singapore, **1998**, p. 385.
[31] A. Laio, M. Parrinello, *Proc. Natl. Acad. Sci. USA* **2002**, *99*, 12562; M. Iannuzzi, A. Laio, M. Parrinello, *Phys. Rev. Lett.* **2003**, *90*, 238302; C. Micheletti, A. Laio, M. Parrinello, *Phys. Rev. Lett.* **2004**, *92*, 170601.
[32] D. J. Earl, M. W. Deem, *Phys. Chem. Chem. Phys.* **2005**, *7*, 3910.
[33] P. G. Bolhuis, *J. Phys. Condens. Matter* **2003**, *15*, S113.
[34] R. Hoffmann, *Angew. Chem.* **1987**, *99*, 871; *Angew. Chem. Int. Ed. Engl.* **1987**, *26*, 846.
[35] N. W. Ashcroft, N. D. Mermin, *Solid State Physics*, Holt, Rinehart & Winston, New York, **1976**.
[36] H. Ibach, H. Lüth, *Solid-State Physics*, 3rd ed., Springer, New York, **2003.**
[37] R. Hoffmann, *Solids and Surfaces: A Chemist's View of Bonding in Extended Structures*, VCH, Weinheim, **1988**.
[38] R. Dronskowski, *Computational Chemistry of Solid State Materials*, Wiley-VCH, Weinheim, **2005**.
[39] P. Brüesch, *Phonons: Theory and Experiments I*, Springer, Berlin, **1982**.

[40] M. I. Aroyo, J. M. Perez-Mato, C. Capillas, E. Kroumova, S. Ivantchev, G. Madariaga, A. Kirov, H. Wondratschek, *Z. Kristallogr.* **2006**, *221*, 15; M. I. Aroyo, A. Kirov, C. Capillas, J. M. Perez-Mato, H. Wondratschek, *Acta Crystallogr. Sect. A* **2006**, *62*, 115.
[41] http://www.cryst.ehu.es.
[42] G. J. Ackland, *J. Phys. Condens. Matter* **2002**, *14*, 2975.
[43] W. C. Swope, H. C. Andersen, P. H. Berens, K. R. Wilson, *J. Chem. Phys.* **1982**, *76*, 637.
[44] We would then practice classical physics, and the thermodynamic properties would result after several million time steps as a statistical mean, in which the absolute temperature runs, without restraint, proportional to the kinetic energy of the atoms: B. J. Alder, T. E. Wainwright, *J. Chem. Phys.* **1957**, *27*, 1208.
[45] R. Haberlandt, S. Fritzsche, G. Peinel, K. Heinzinger, *Molekulardynamik*, Vieweg, Braunschweig, **1995**.
[46] Indeed this succeeds, owing to the purely coincidental crossing of the phase space, only over an extremely large number of structural configurations: N. Metropolis, A. W. Rosenbluth, M. N. Rosenbluth, A. H. Teller, E. Teller, *J. Chem. Phys.* **1953**, *21*, 1087.
[47] E. Schrödinger, *Ann. Phys.* **1926**, *79*, 361.
[48] P. A. M. Dirac, *Proc. R. Soc. London Ser. A* **1928**, *117*, 610; P. A. M. Dirac, *Proc. R. Soc. London Ser. A* **1928**, *118*, 315.
[49] M. Born, R. Oppenheimer, *Ann. Phys.* **1927**, *84*, 457.
[50] I. N. Levine, *Quantum Chemistry*, 5th ed., Prentice Hall, Englewood Cliffs, **2000**.
[51] A. Szabo, N. S. Ostlund, *Modern Quantum Chemistry: Introduction to Advanced Electronic Structure Theory*, McGraw-Hill, New York, **1989**.
[52] W. Kutzelnigg, *Einführung in die Theoretische Chemie*, Wiley-VCH, Weinheim, **1993**.
[53] F. Jensen, *Introduction to Computational Chemistry*, Wiley, New York, **1999**.
[54] C. J. Cramer, *Essentials of Computational Chemistry*, repr., Wiley, New York, **2004**.
[55] F. Bloch, *Z. Phys.* **1928**, *52*, 555
[56] Tight-binding procedure: J. Bullett, *Solid State Phys.* **1980**, *35*, 215.
[57] Semi-empirical extended Hückel method: R. Hoffmann, *J. Chem. Phys.* **1963**, *39*, 1397; R. Hoffmann, *J. Chem. Phys.* **1964**, *40*, 2745; R. Hoffmann, *J. Chem. Phys.* **1964**, *40*, 2474.
[58] Ab initio approach based on Gaussian functions according to Hartree–Fock: C. Pisani, R. Dovesi, *Int. J. Quantum Chem.* **1980**, *17*, 501; V. R. Saunders, *Faraday Symp. Chem. Soc.* **1984**, *19*, 79; C. Pisani, R. Dovesi, C. Roetti, *Lect. Notes Chem.*, *Vol. 48*, Springer, Heidelberg, **1988**.
[59] FPLO method: K. Koepernik, H. Eschrig, *Phys. Rev. B* **1999**, *59*, 1743; I. Opahle, K. Koepernik, H. Eschrig, *Phys. Rev. B* **1999**, *60*, 14035.
[60] TB-LMTO-ASA method: O. K. Andersen, O. Jepsen, *Phys. Rev. Lett.* **1984**, *53*, 2571.
[61] "Linearized" electronic-structure methods: O. K. Andersen, *Phys. Rev. B* **1975**, *12*, 3060.
[62] P. Pulay, *Mol. Phys.* **1969**, *17*, 197.
[63] H. Hellmann, *J. Chem. Phys.* **1935**, *3*, 61; H. Hellmann, *Acta Physicochim. URSS* **1934**, *1*, 913; H. Hellmann, *Acta Physicochim. URSS* **1936**, *4*, 225.
[64] K. Balasubramanian in *Encyclopedia of Computational Chemistry*, *Vol. 4* (Eds.: P. v. R. Schleyer et al.), Wiley, New York, **1998**.
[65] L. Seijo, Z. Barandiarán in *Computational Chemistry, Reviews of Current Trends*, *Vol. 4* (Ed.: J. Leszczynski), World Scientific, Singapore, **1999**.
[66] M. Dolg in *Modern Methods and Algorithms of Quantum Chemistry*, *NIC Series*, *Vol. 3* (Ed.: J. Grotendorst), John von Neumann Institute for Computing, Jülich, **2000**.
[67] M. Dolg in *Relativistic Electronic Structure Theory, Part I: Fundamentals, Theoretical and Computational Chemistry*, *Vol. 11* (Ed.: P. Schwerdtfeger), Elsevier, Amsterdam, **2002**.
[68] W. A. Harrison, *Pseudopotentials in the Theory of Metals*, Benjamin, New York, **1966**.
[69] A. Zunger, M. Cohen, *Phys. Rev. B* **1978**, *18*, 5449.
[70] D. R. Hamann, M. Schlüter, C. Chiang, *Phys. Rev. Lett.* **1979**, *43*, 1494.
[71] L. Kleinman, D. M. Bylander, *Phys. Rev. Lett.* **1982**, *48*, 1425.
[72] G. B. Bachelet, D. R. Hamann, M. Schlüter, *Phys. Rev. B* **1982**, *26*, 4199.
[73] D. Vanderbilt, *Phys. Rev. B* **1985**, *32*, 8412.
[74] N. Troullier, J. L. Martins, *Solid State Commun.* **1990**, *74*, 613.
[75] X. Gonze, R. Stumpf, M. Scheffler, *Phys. Rev. B* **1991**, *44*, 8503.
[76] M. Fuchs, M. Scheffler, *Comput. Phys. Commun.* **1999**, *119*, 67.
[77] S. Goedecker, M. Teter, J. Hutter, *Phys. Rev. B* **1996**, *54*, 1703.
[78] C. Hartwigsen, S. Goedecker, J. Hutter, *Phys. Rev. B* **1998**, *58*, 3641.
[79] D. Vanderbilt, *Phys. Rev. B* **1990**, *41*, 7892.
[80] P. E. Blöchl, *Phys. Rev. B* **1994**, *50*, 17953.
[81] G. Kresse, J. Hafner, *J. Phys. Condens. Matter* **1994**, *6*, 8245; G. Kresse, J. Furthmüller, *Comput. Mater. Sci.* **1996**, *6*, 15; G. Kresse, J. Furthmüller, *Phys. Rev. B* **1996**, *54*, 11169.
[82] J. Hafner, *J. Comput. Chem.* **2008**, *29*, 2044.
[83] R. A. Evarestov, A. V. Bandura, M. V. Losev, E. A. Kotomin, Y. F. Zhukovskii, D. Bocharov, *J. Comput. Chem.* **2008**, *29*, 2079.
[84] R. G. Parr, W. Yang, *Density Functional Theory of Atoms and Molecules*, Clarendon, New York, **1989**.
[85] R. O. Jones, O. Gunnarsson, *Rev. Mod. Phys.* **1989**, *61*, 689.
[86] W. Koch, M. C. Holthausen, *A Chemist's Guide to Density Functional Theory*, 2nd ed., Wiley-VCH, Weinheim, **2001**.
[87] P. Hohenberg, W. Kohn, *Phys. Rev.* **1964**, *136*, B864.
[88] W. Kohn, L. J. Sham, *Phys. Rev.* **1965**, *140*, A1133.
[89] V. Fock, *Z. Phys.* **1930**, *61*, 126; V. Fock, *Z. Phys.* **1930**, *62*, 795.
[90] M. J. Gillan, D. Alfè, S. de Gironcoli, F. R. Manby, *J. Comput. Chem.* **2008**, *29*, 2098.
[91] C. Pisani, L. Maschio, S. Casassa, M. Halo, M. Schütz, D. Usvyat, *J. Comput. Chem.* **2008**, *29*, 2113.
[92] C. Møller, M. S. Plesset, *Phys. Rev.* **1934**, *46*, 618.
[93] U. von Barth, L. Hedin, *J. Phys. C* **1972**, *5*, 1629.
[94] S. H. Vosko, L. Wilk, M. Nusair, *Can. J. Phys.* **1980**, *58*, 1200.
[95] J. P. Perdew, Y. Wang, *Phys. Rev. B* **1992**, *45*, 13244.
[96] J. P. Perdew, S. Burke, M. Ernzerhof, *Phys. Rev. Lett.* **1996**, *77*, 3865.
[97] J. P. Perdew, K. Burke, Y. Wang, *Phys. Rev. B* **1996**, *54*, 16533.
[98] T. J. Frankcombe, G.-J. Kroes, *Phys. Rev. B* **2006**, *73*, 174302.
[99] Gmelin *Handbuch der Anorganischen Chemie*, 8th ed., Verlag Chemie, Weinheim, **1955**.
[100] W. Frank, C. Elsässer, M. Fähnle, *Phys. Rev. Lett.* **1995**, *74*, 1791.
[101] K. Parlinski, Z. Q. Li, Y. Kawazoe, *Phys. Rev. Lett.* **1997**, *78*, 4063.
[102] H. Hellmann, *Einführung in die Quantenchemie*, Franz Deuticke, Leipzig, **1937**.
[103] R. P. Feynman, *Phys. Rev.* **1939**, *56*, 340.
[104] X. Gonze, *Phys. Rev. B* **1997**, *55*, 10337; X. Gonze, C. Lee, *Phys. Rev. B* **1997**, *55*, 10355.
[105] F. D. Murnaghan, *Proc. Natl. Acad. Sci. USA* **1944**, *30*, 244.
[106] F. Birch, *Phys. Rev.* **1947**, *71*, 809.
[107] H. J. Monkhorst, J. D. Pack, *Phys. Rev. B* **1976**, *13*, 5188.
[108] N. D. Mermin, *Phys. Rev. A* **1965**, *137*, 1441.
[109] Luckily, reciprocal space directly contracts with the expansion of real space, so that the net of *k*-points may become

accordingly coarser. Assuming sufficiently large supercells, electron-theory computations sometimes are adequately precise even at a single point of reciprocal space: D. J. Chadi, M. L. Cohen, *Phys. Rev. B* **1973**, *8*, 5747.
[110] V. H. Vetter, R. A. Bartels, *J. Phys. Chem. Solids* **1973**, *34*, 1448.
[111] http://www.mem-brain-allianz.de.
[112] Yu. N. Pivovarov, V. Ya. Dashevskii, *Russ. Metall.* **2006**, *4*, 286.
[113] G. O. Brunner, D. Schwarzenbach, *Z. Kristallogr.* **1971**, *133*, 127.
[114] Z. Shao, S. M. Haile, *Nature* **2004**, *431*, 170.
[115] R. Nast, H. Schindel, *Z. Anorg. Allg. Chem.* **1963**, *326*, 201.
[116] R. Nast, *Coord. Chem. Rev.* **1982**, *47*, 89.
[117] U. Ruschewitz, unpublished results.
[118] The IR spectrum of $Ag[Ag(C_3H_3)_2]$ was provided by Prof. Dr. Uwe Ruschewitz (Universität zu Köln) and published with gracious permission.
[119] M. Hesse, H. Meier, B. Zeeh, *Spektroskopische Methoden in der Organischen Chemie*, 5th ed, Georg Thieme Verlag, Stuttgart, **1995**.
[120] A. F. Wells, *Structural Inorganic Chemistry*, 5th ed., Oxford University Press, Oxford, **1984**.
[121] U. Müller, *Inorganic Structural Chemistry*, Wiley, New York, **1993**.
[122] I. N. Nikolaev, V. P. Marin, V. W. Panyushkin, L. S. Pavlyukov, *Sov. Phys. Solid State* **1973**, *14*, 2022.
[123] J. von Appen, K. Hack, R. Dronskowski, *J. Alloys Compd.* **2004**, *379*, 110.
[124] The computational expense would increase immediately by a factor of 10^5 if we could not radically reduce the number of k points at the same time.
[125] A. F. Holleman, E. Wiberg, *Lehrbuch der Anorganischen Chemie*, 101st ed., Walter de Gruyter, Berlin, **2007**.
[126] R. Marchand, Y. Laurent, J. Guyader, P. l'Haridon, P. Verdier, *J. Eur. Ceram. Soc.* **1991**, *8*, 197.
[127] R. Metselaar, *Pure Appl. Chem.* **1994**, *66*, 1815.
[128] M. Jansen, H. P. Letschert, *Nature* **2000**, *404*, 980.
[129] Y.-I. Kim, P. M. Woodward, K. Z. Baba-Kishi, C. W. Tai, *Chem. Mater.* **2004**, *16*, 1267.
[130] K. Miga, K. Stanczyk, C. Sayag, D. Brodzki, G. Djéga-Mariadassou, *J. Catal.* **1999**, *183*, 63.
[131] G. Hitoki, T. Takata, J. N. Kondo, M. Hara, H. Kobayashi, K. Domen, *Chem. Commun.* **2002**, 1698.
[132] G. Brauer, J. R. Weidlein, *Angew. Chem.* **1965**, *77*, 913; *Angew. Chem. Int. Ed. Engl.* **1965**, *4*, 875.
[133] G. Brauer, J. R. Weidlein, J. Strähle, *Z. Anorg. Allg. Chem.* **1966**, *348*, 298.
[134] D. Armytage, B. E. F. Fender, *Acta Crystallogr. Sect. B* **1974**, *30*, 809.
[135] M.-W. Lumey, R. Dronskowski, *Z. Anorg. Allg. Chem.* **2003**, *629*, 2173.
[136] M.-W. Lumey, R. Dronskowski, *Z. Anorg. Allg. Chem.* **2005**, *631*, 887.
[137] H. Schilling, A. Stork, E. Irran, H. Wolff, T. Bredow, R. Dronskowski, M. Lerch, *Angew. Chem.* **2007**, *119*, 2989; *Angew. Chem. Int. Ed.* **2007**, *46*, 2931.
[138] H. Wolff, T. Bredow, M. Lerch, H. Schilling, E. Irran, A. Stork, R. Dronskowski, *J. Phys. Chem. A* **2007**, *111*, 2745.
[139] P. A. Fleury, *Annu. Rev. Mater. Sci.* **1976**, *6*, 157.
[140] J. G. Bednorz, K. A. Müller, *Z. Phys. B* **1986**, *64*, 189.
[141] M. K. Wu, R. J. Ashburn, C. J. Torng, P. H. Hor, R. L. Meng, L. Gao, Z. J. Huang, Y. Q. Wang, C. W. Chu, *Phys. Rev. Lett.* **1987**, *58*, 908.
[142] *High T_C Superconductors and Related Transition Metal Oxides* (Eds.: A. Bussmann-Holder, A. Keller), Springer, Berlin, **2007**.
[143] R. J. Cava, *J. Am. Ceram. Soc.* **2000**, *83*, 5.
[144] A. Simon, K. Trübenbach, H. Borrmann, *J. Solid State Chem.* **1993**, *106*, 128.
[145] R. J. Cava, A. W. Hewat, E. A. Hewat, B. Batlogg, M. Marezio, K. M. Rabe, J. J. Krajewski, W. F. Peck, L. W. Rupp, Jr., *Physica C* **1990**, *165*, 419.
[146] M. Bäcker, T. Schneller, *Nachr. Chem.* **2007**, *55*, 1202.
[147] G. F. Voronin, *Pure Appl. Chem.* **2000**, *72*, 463.
[148] R. Car, M. Parrinello, *Phys. Rev. Lett.* **1985**, *55*, 2471.
[149] B. Grabowski, L. Ismer, T. Hickel, J. Neugebauer, *Phys. Rev. B* **2009**, *79*, 134106.
[150] M. Gilleßen, R. Dronskowski, *J. Comput. Chem.* **2009**, *30*, 1290.
[151] Y. Kurtulus, R. Dronskowski, G. Samolyuk, V. P. Antropov, *Phys. Rev. B* **2005**, *71*, 014425; Y. Kurtulus, M. Gilleßen, R. Dronskowski, *J. Comput. Chem.* **2006**, *27*, 90.
[152] M. A. Uijttewaal, T. Hickel, J. Neugebauer, M. E. Gruner, P. Entel, *Phys. Rev. Lett.* **2009**, *102*, 035702.
[153] X. Liu, P. Müller, P. Kroll, R. Dronskowski, W. Wilsmann, R. Conradt, *ChemPhysChem* **2003**, *4*, 725.
[154] S. Grimme, *J. Comput. Chem.* **2006**, *27*, 1787.
[155] P. Fulde, *Electron Correlations in Molecules and Solids*, 2nd ed., Springer, Berlin, **1993**.
[156] V. I. Anisimov, F. Aryasetiawan, A. I. Liechtenstein, *J. Phys. Condens. Matter* **1997**, *9*, 767.
[157] S. L. Dudarev, G. A. Botton, S. Y. Savrasov, C. Humphreys, A. P. Sutton, *Phys. Rev. B* **1998**, *57*, 1505.
[158] S. Grimme, *Angew. Chem.* **2006**, *118*, 4571; *Angew. Chem. Int. Ed.* **2006**, *45*, 4460.
[159] A. M. Tokmachev, R. Dronskowski, *Phys. Rev. B* **2005**, *71*, 195202; A. M. Tokmachev, R. Dronskowski, *Chem. Phys.* **2006**, *322*, 423; A. L. Tchougréeff, A. M. Tokmachev, R. Dronskowski, *J. Phys. Chem. A* **2009**, *113*, 11406.
[160] A. L. Tchougréeff, *Hybrid Methods of Molecular Modeling*, Springer, Berlin, **2008**.
[161] A. R. Oganov, S. Ono, *Nature* **2004**, *430*, 445.
[162] D. M. Ceperley, B. I. Alder, *Phys. Rev. Lett.* **1980**, *45*, 566; parametrized by J. P. Perdew, A. Zunger, *Phys. Rev. B* **1981**, *23*, 5048.
[163] B. Eck, *wxDragon 1.3*, RWTH Aachen, **1994–2009**.
[164] A. Togo, *Fropho: A Tool to Compute Phonon Band Structures and Thermal Properties of Solids*, RWTH Aachen University, **2007–2008**. Available at http://fropho.sourceforge.net.
[165] A. Togo, F. Oba, I. Tanaka, *Phys. Rev. B* **2008**, *78*, 134106.
[166] R. Stoffel, Dissertation in preparation, RWTH Aachen, **2008–2010**.
[167] T. C. Ozawa, S. J. Kang, *J. Appl. Crystallogr.* **2004**, *37*, 679.
[168] R. De Souza, M. Martin, *Monatsh. Chem.* **2009**, *140*, 1011.

